










METHODOLOGY

Open Access



From freeze to function: optimised cryopreservation and mitochondrial analysis workflow for skeletal muscle biopsies

Maheen Wahid^{1*} , Graeme Mackenzie¹, Liam M. Rooney¹ , Justin C. Greig¹ , Gail McConnell¹ ,
Emilie Combet² , Stuart Gray³ , James T. Murray⁴ , Susan Currie¹, Gwyn W. Gould¹  and
Margaret R. Cunningham^{1*} 

Abstract

Background Skeletal muscle biopsies are valuable in clinical and research settings, contributing to advancements in diagnosing, understanding, and treating muscle-related conditions. Traditional freezing methods often cause artefacts mistaken for disease, leading to incorrect diagnoses or misinterpretation of research findings. Proper handling of muscle biopsies is critical for accurate histopathological and mitochondrial analysis. It is essential to preserve the entire tissue, especially for small needle biopsies. While most research focuses on mitochondrial analysis in cells, there are few studies on whole tissue samples. This study aimed to provide an effective methodological workflow to improve cryopreservation techniques for human and rodent muscle biopsies and create a reliable method for mitochondrial analysis in muscle tissues.

Methods Human muscle samples were preserved with different concentrations of formaldehyde after freezing with liquid nitrogen to study the effects of freeze–thaw cycles. We compared the edge and belly of muscle samples embedded in Optimal Cutting Temperature compound (OCT) to see how OCT affects ice crystal formation. Rat muscle biopsies were frozen using six different methods, using liquid nitrogen and precooled isopentane as freezing media. Each medium involved direct immersion, OCT dip before immersion, and placement in histocassettes before immersion. Effectiveness of these methods was evaluated using histological and immunohistochemical staining. Mitochondrial analysis in type I and II myofibres was attempted by employing the Trainable Weka Segmentation plugin using Fiji.

Results Histologically stained human tissue sections showed that freeze–thaw and formaldehyde fixation led to freezing artefacts, disrupted endomysium, and widely spaced cells. Quantitative differences in ice crystal artefacts between edge and belly of rat whole muscle samples demonstrated effects of OCT in crystal formation. Histological and immunohistochemical staining of sections from rat muscle biopsies frozen in six different cryopreservation techniques revealed that only isopentane/histocassette combination preserved tissue integrity in both core and periphery of tissue sections. Moreover, an optimised Fiji workflow enabled accurate quantification and mapping of mitochondrial networks.

*Correspondence:

Maheen Wahid
maheen.wahid.2022@uni.strath.ac.uk
Margaret R. Cunningham
margaret.cunningham@strath.ac.uk

Full list of author information is available at the end of the article



© The Author(s) 2024. **Open Access** This article is licensed under a Creative Commons Attribution 4.0 International License, which permits use, sharing, adaptation, distribution and reproduction in any medium or format, as long as you give appropriate credit to the original author(s) and the source, provide a link to the Creative Commons licence, and indicate if changes were made. The images or other third party material in this article are included in the article's Creative Commons licence, unless indicated otherwise in a credit line to the material. If material is not included in the article's Creative Commons licence and your intended use is not permitted by statutory regulation or exceeds the permitted use, you will need to obtain permission directly from the copyright holder. To view a copy of this licence, visit <http://creativecommons.org/licenses/by/4.0/>.

Discussion The isopentane/histocassette combination is an effective cryopreservation method, ensuring artefact-free preservation of both core and periphery of tissue sections. Our workflow utilising Trainable Weka Segmentation plugin provides a reliable method for mitochondrial analysis in skeletal muscle tissues, facilitating future studies in muscle research.

Keywords Skeletal muscle biopsy, Sample handling, Processing, Storage, Imaging, Mitochondria, Analysis

Introduction

Skeletal muscle biopsies play a critical role in advancing research across both fundamental and applied life sciences. In ageing research, skeletal muscle biopsies can provide insight into age-associated changes in muscle architecture, metabolism and function, for example providing mechanistic insight on sarcopenia [1]. Muscle biopsies are indispensable tools for understanding neuromuscular disorders, providing diagnostic evidence and allowing disease characterisation [2]. Moreover, skeletal muscle biopsies are pivotal in exercise and sports science, aiding researchers in investigating the effects of training activities and nutritional interventions [3, 4]. The comprehensive analysis of tissue obtained via biopsies can help elucidate different mechanisms underlying physiological and pathophysiological conditions, ultimately aiding in formulating strategies to enhance muscle health and performance across the lifespan.

The fragility of skeletal muscle samples highlights the importance of meticulous handling protocols, a practice supported by numerous studies in literature [5–8]. Muscle tissue is extremely susceptible to freezing artefacts that can distort histopathological features within the sample and compromise findings. These artefacts can be misinterpreted and hence, give rise to misleading diagnoses [5]. Moreover, inappropriate handling of skeletal muscle biopsies can not only lead to loss of valuable samples, but also warrant the need for resampling. This can become cumbersome in studies involving large cohorts or rare patient populations, which may cause stress and discomfort to patients and lead to additional unseen costs with the need to repeat poor-quality samples. Whilst existing literature offers various cryopreservation protocols [5–8], needle biopsies are limited in size, and require a method that can effectively preserve both core and peripheral regions of the tissue section. Therefore, optimising handling techniques to minimise freezing artefacts in the entirety of the sample, preventing subsequent loss of sample and experimental failure, is important to ensure the reliability of histopathological analyses, and to support more robust scientific interpretations in studies of muscle physiology, pathology and bioenergetics.

The ability to detect skeletal muscle mitochondrial dynamics and pathological remodelling has long been

an area of intense research interest. Mitochondria play a crucial role in skeletal muscle bioenergetics, making them vital to muscle function. With ageing, skeletal muscle bioenergetics undergo degenerative changes, attributed to mitochondrial dysfunction and this can contribute to sarcopenia [9]. Therefore, comprehensive mitochondrial analysis is imperative to fully understand changes in muscle energetics in different conditions, such as ageing. Fiji, an open-source image analysis software, is often used for quantitative investigation of the mitochondrial network [10]. While multiple Fiji plugins for mitochondrial analysis exist in the cell biology literature [11, 12], implementing these is challenging with tissue samples. Most mitochondrial dyes stain living cells. Those that can be employed for tissues, such as MitoView Green and IraZolve-Mito, lead to high background noise, hindering accurate quantitative analysis [13, 14]. As a result, existing plugins may not effectively delineate mitochondrial morphology in tissue samples, distorting the accurate capture and analysis of mitochondrial networks. This gap in the published literature hinders a comprehensive understanding of mitochondrial (dys)function. While a substantial body of literature exists on various aspects of skeletal muscle biology, including ageing, neuromuscular disorders, exercise physiology and mitochondrial dysfunction, navigating through this literature can be laborious, particularly when troubleshooting and problem-solving in an experimental setting. Therefore, developing and optimising a workflow in Fiji that specifically addresses these challenges is crucial for advancing mitochondrial analysis in the context of various conditions, such as ageing.

This study aims to provide a methodological pipeline to support researchers and clinicians involved in skeletal muscle research by optimising cryopreservation techniques, addressing freezing artefacts, and refining mitochondrial analysis methodologies.

Methods

Study design and rationale

Human and rodent skeletal muscle samples are commonly used in investigations encompassing both research and diagnostic purposes. The study was designed to develop a workflow for best practices to support researchers, especially those new to the handling of

skeletal muscle samples. Here, we address the entire process from cryopreservation to imaging for morphological features and staining for various markers indicative of changes in cellular architecture. We focused on quantifying artefacts and functional organelles that provide insight into muscle physiology. The experimental protocols used in this study tackle common issues and offer solutions to challenges associated with tissue processing. By providing practical solutions to data analysis challenges, this study provides a framework for a more accurate assessment of skeletal muscle samples in both research and diagnostic contexts, ultimately contributing to advancements in understanding muscle bioenergetics and pathology.

Methods for specimen handling optimisation

All materials used can be found in the Supplementary Material section (Supplementary Tables 1–3).

Healthy human volunteers

Muscle biopsy samples (~ 50 mg) were collected from the vastus lateralis muscle, under local anaesthesia, using an automatic biopsy needle (Bard, 12 gauge). Samples were rinsed with sterile saline and dissected free from any fat or connective tissue before being snap-frozen in liquid nitrogen (LN₂). Samples were then stored at -80 °C before subsequent analysis. These samples were collected as part of another study [15]. The biopsies were collected by Prof Stuart Gray, a co-author for both the current and cited study, and the use of these samples in the current study for microscopy analysis was ethically approved by the College of Medical, Veterinary and Life Sciences Ethical Committee at the University of Glasgow (Approval No. 200150044). Participants provided written informed consent prior to participation in the original study. No additional ethics approval was required for the current study, as the use of the samples for microscopy falls under the scope of the original ethical approval.

Supplemental tables are included that detail specific methodologies for the processing for human muscle biopsy samples (Supplementary Table 4).

Animal procedures

Adult male Sprague Dawley rats, 8–12 weeks of age, weighing 250–300 g were purchased from the Biological Procedures Unit (BPU) at the Strathclyde Institute of Pharmacy and Biomedical Sciences, University of Strathclyde, Glasgow. The animals were housed in cages of up to 4 rats, within the Home Office Code of Practice Stocking Density, on a cycle of 12 h light/12 h dark, with access to a standard chow diet and purified water. All animals were handled in strict accordance with good animal practice approved by The Animals in Science Regulation Unit.

Each procedure was performed under sterile conditions and adapted by the Guide for the Care and Use of Laboratory Animals published by the US National Institutes of Health (NIH Publication No. 85–23, revised 1996) and Directive 2010/63/EU of the European Parliament. The rats were euthanised by cervical dislocation, followed by secondary confirmation of death by femoral artery severance. Samples were taken from gastrocnemius and vastus lateralis muscles. Cryopreservation procedures were carried out on both whole muscles and biopsy samples.

Supplemental tables are included that detail specific methodologies for the processing for rodent muscle biopsy samples (Supplementary Table 4).

Cryopreservation

Muscle samples were handled consistently to ensure uniform freezing. For immersion in liquid nitrogen (LN₂), samples were carefully held using forceps at the edge, ensuring minimal handling and avoiding contact with the belly of the muscle. Importantly, the same edge used for handling was mounted on the metal disc holder of the cryostat, ensuring that the opposite edge remained untouched and unmanipulated. Muscle samples were immersed in a dewar containing LN₂ for 10 to 15 s. For samples preserved using an isopentane cryopreservation technique, isopentane was added to a beaker mounted on a ladle and immersed in LN₂, ensuring that the level of isopentane was below the level of LN₂. Once the bottom surface of the pre-cooled isopentane beaker turned white (opaque white ‘pearls’ are visible), the samples were similarly handled as before, ensuring belly and one edge remain untouched by forceps. The specimen was immersed in pre-cooled isopentane for 10 to 15 s. The samples were then transferred to 1.5 mL tubes pre-cooled in dry ice using prechilled forceps, and stored at -80 °C. This process was repeated for rat whole muscle samples embedded in OCT, and smaller rat biopsy samples placed in a histocassette or dipped in Optimal Cutting Temperature (OCT) compound before immersion in LN₂ or pre-cooled isopentane. Consistent positioning was maintained to standardize the freezing process.

Cryosectioning and slide preparation

A Leica CM1950 clinical cryostat was used for sectioning. The chamber temperature was set at -25 °C and the specimen head temperature was set at -20 °C. Forceps, metal object holder discs and the muscle sample within a cryovial or cryomold were all placed in the cryostat for 30 min to allow temperature equilibration. A new microtome blade was used for each cryotome procedure. Whole muscle samples preserved in LN₂ were placed on the metal holder discs and layered with OCT before sectioning. For sectioning without OCT, only a thin layer of

OCT was applied to the base of the specimen to allow adherence to the metal disc. Care was taken to handle samples by the edge, with the same edge being used for mounting on the disc as was held with forceps in the cryopreservation process to avoid damage to other regions. All samples were held using prechilled forceps to eliminate any source of freeze–thaw.

Tissue was sectioned at a thickness of 8 μm and transferred onto SuperFrost slides kept at room temperature to ensure optimal tissue adhesion to the slide surface. The slides were stored at $-80\text{ }^{\circ}\text{C}$, and when needed for histological or immunohistochemical staining procedures, were taken out of the freezer, and left at room temperature overnight one day before the experiment.

Fluorescence microscopy and immunohistochemistry

The tissue sections on microscope slides were circled with an ImmEdge(R) hydrophobic barrier PAP pen (Vector Laboratories, H-4000), and washed twice in Phosphate Buffered Saline (PBS) for 5 min, followed by fixation in 3.6% (v/v) formaldehyde in PBS for 10 min. After two subsequent washes with PBS, the sections were placed in 0.25% (v/v) Triton X-100 in PBS for 10 min, and then washed twice with PBS. The sections were then blocked using 1% (w/v) Bovine Serum Albumin (BSA) in PBS for 1 h, after which 50 μL of Voltage Dependent Anion Channel (VDAC) VDAC1/Porin + VDAC 3 anti-mouse monoclonal antibody (1:200, details in Table 2) was added to each section. The section was placed in the dark for overnight incubation at $4\text{ }^{\circ}\text{C}$. The next day, the antibody was aspirated, and the sections were washed three times with PBS (for 5 min per wash) directly on the slide. After incubation in blocking buffer for 30 min, Alexa Fluor 555 goat anti-mouse IgG was added to the tissue and incubated for 2 h in the dark, before the sections were washed three times in PBS.

When staining for mitochondria, MitoView Green (100 nM, in PBS) was added to the sections for 20 min, and then washed three times in PBS.

Final staining with 4',6-diamidino-2-phenylindole (DAPI) and Rhodamine-phalloidin (1:2000 and 1:40 respectively) was carried out. After a 20-min incubation with the dyes, the sections were washed three more times with PBS, and the slides were mounted in Vector Mount aqueous mounting medium with a cover slip. Images were acquired using a Leica SP8 confocal laser scanning microscope (with Leica Application Suite X software).

Picrosirius red staining

To assess the morphological and structural integrity of the tissue sections, Picrosirius Red Staining (PSR) staining was performed. After washing off the OCT twice with PBS, tissue sections were fixed in 3.6% (v/v)

formaldehyde in PBS for 10 min, followed by another two washes with PBS. A hydrophobic barrier pen was used to draw around tissue sections as previously described. PSR stain (50 μL) was then added to each section and the slides were incubated for 1 h at room temperature. The sections were then rinsed in acetic acid twice and dehydrated in two changes of absolute ethanol. The aforementioned steps were the same for tissues sectioned without OCT, to ensure uniformity in protocol. Lastly, the sections were mounted in Histomount mounting medium and sealed with glass coverslip.

Haematoxylin & eosin staining

To assess the morphological and structural integrity of the tissue sections, Haematoxylin & Eosin (H&E) staining was performed. Tissue sections were rinsed twice with PBS, and then fixed in 3.6% (v/v) formaldehyde in PBS for 10 min, followed by another two washes with PBS. A hydrophobic barrier pen was used to draw around tissue sections as previously described. Haematoxylin stain (50 μL) was then added to each section and the slides were incubated for 5 min at room temperature. The sections were then rinsed in distilled water twice and incubated with Bluing's reagent for 15 s. The slides were rinsed in two changes of distilled water and dipped once in absolute alcohol. This was followed by the addition of 50 μL Eosin stain to each section for 3 min. The sections were then dehydrated in four changes of absolute ethanol. Lastly, the sections were mounted in Histomount mounting medium and sealed with glass coverslip.

Oil red o staining

A hydrophobic barrier pen was used to draw around each tissue section. The sections were then fixed in 10% (v/v) formalin in water for 5 min. Following aspiration, the sections were incubated in 10% (v/v) formalin in distilled water for another 60 min. Then, 60% (v/v) isopropanol in distilled water was added once for 30 s and aspirated. The slides were briefly air dried, and then incubated with Oil O Red (ORO) working solution for 10 min. The slides were then washed four times with distilled water. Lastly, the sections were mounted in Histomount mounting medium and sealed with glass coverslip.

Imaging

Brightfield imaging

PSR, H&E and ORO-stained tissue were visualized using EVOS FL Auto microscope using 20x/0.4NA (air) objective lens. For stitched images, a 3 \times 3 tiled image was created using sequential scanning, and saved as a.PNG file. All images were analysed using Fiji [10].

Confocal imaging

Fluorescence microscopy images were obtained via a Leica SP8 confocal laser scanning microscope. Fluorescence emission was acquired using a 63x/1.4NA (oil) objective lens and detected using a photomultiplier tube with spectral gating according to the respective fluorophores. Laser excitation was provided at 405 nm (DAPI), 488 nm (MitoView Green) and 552 nm (Rhodamine-phalloidin/VDAC). For z-stacks, the step size was set at the Nyquist rate using the 'optimal' setting on the Leica Application Suite X software. All images were saved as .LIF files, processed using Fiji, and saved as .png files.

Ice crystal analysis

The ice crystal analysis was performed using images of PSR-stained tissue in Fiji. A region of interest (ROI) was drawn and saved for all subsequent image analysis. ROI was cropped and converted to an 8-bit type image to permit thresholding to select the ice crystals from the dark background (i.e., PSR-stained tissue). The Analyse Particles function was used to obtain the area fraction occupied by the ice crystals. Four ROIs were calculated as above for both core and peripheral regions for sections taken from either the edge or belly of skeletal muscle whole muscle samples. This was done for two biological replicates. The mean area fraction was plotted as a percentage of the tissue area occupied by ice crystals for each group as a bar graph in GraphPad Prism.

Mitochondrial analysis

Four ROIs were drawn using Fiji for each fibre type from the image and mitochondrial footprint, mean branch length, mean summed branch length, and mean network branches were obtained from the MiNA plugin [16]. The mean of each parameter was plotted as a bar graph in GraphPad Prism. The mitochondrial workflow is described in detail in the results section.

Statistical analysis

All statistical analysis was performed using GraphPad Prism version 8. The normality of data was assessed using the Shapiro–Wilk test. Normally distributed data was presented as mean with standard deviation (SD) and analysed using an unpaired t-test. Skewed data was presented as the median with an interquartile range (IQR) and a Mann Whitney-U test was employed for statistical analysis. P-values < 0.05 were considered significant for all statistical tests.

Results

Specimen handling optimisation – human samples

The first experiments were conducted on human skeletal muscle biopsies obtained from the vastus lateralis muscle

via an automatic biopsy needle (Bard, 12 gauge), frozen in LN₂. Samples were first subjected to various preservation techniques before cryosectioning to assess the best approach.

Two samples were directly embedded in OCT in a cryomold before cryosectioning. For two samples, fixation with formaldehyde was attempted at concentrations of 10% and 36% in PBS, before being embedded in OCT and subsequent cryosectioning. Two samples were refrozen in LN₂ and embedded in OCT prior to cryosectioning. The OCT was allowed to freeze while sitting in dry ice. PSR staining following cryosectioning was done to assess structural morphology. Images were visualised under an EVOS brightfield microscope. PSR stains the cells yellow, and collagen (part of connective tissue—perimysium/endomysium) appears red, but some PSR tissue sections stained red completely. However, the stained tissues still provided an accurate representation of the shape of cells, and showed whether there was any disruption in encapsulating connective tissue layers.

Preservation of skeletal muscle biopsies with various conditions demonstrated a wide spectrum of outcomes, and we examined the PSR-stained tissue to assess whether normal skeletal muscle structure (Fig. 1a) is preserved. Complete disintegration of tissue with only connective tissue streaks was visible, and randomly arranged cells with no distinction between fascicles was observed with direct OCT embedment (Fig. 1b), formaldehyde concentration of 10% (Fig. 1c) and refreezing in LN₂ (Fig. 1d). The existing literature advises against the use of fixatives for histological and immunohistochemical staining [5, 17, 18]. However, of all the methods tried on the human skeletal muscle biopsies, fixation with 36% formaldehyde showed the best preservation of structure and morphology (Fig. 1e). In early optimisation studies, the biopsy samples disintegrated at lower concentrations of formaldehyde, irrespective of temperature.

A closer inspection of the extent of structural preservation of samples fixed in 36% formaldehyde (Fig. 2a) showed that the cells appeared widely spaced out, with inadequate clustering to form fascicles. The perimysium, although present at the demarcation between fascicles, appeared disrupted, as opposed to how myofibre organisation should appear – as tightly apposed cells, packed within well-demarcated fascicles, with the dividing perimysium [19]. The endomysium, usually indiscernible due to the tight juxtaposition of myofibres, could be seen streaking between cells. Wide spacing of cells can be observed due to handling artefacts, when the tissue is either dried out before preservation, or immersed in saline for too long [20]. We considered the likelihood of specimen handling artefacts. Results of ORO staining are shown in Fig. 2b, displaying the presence of large

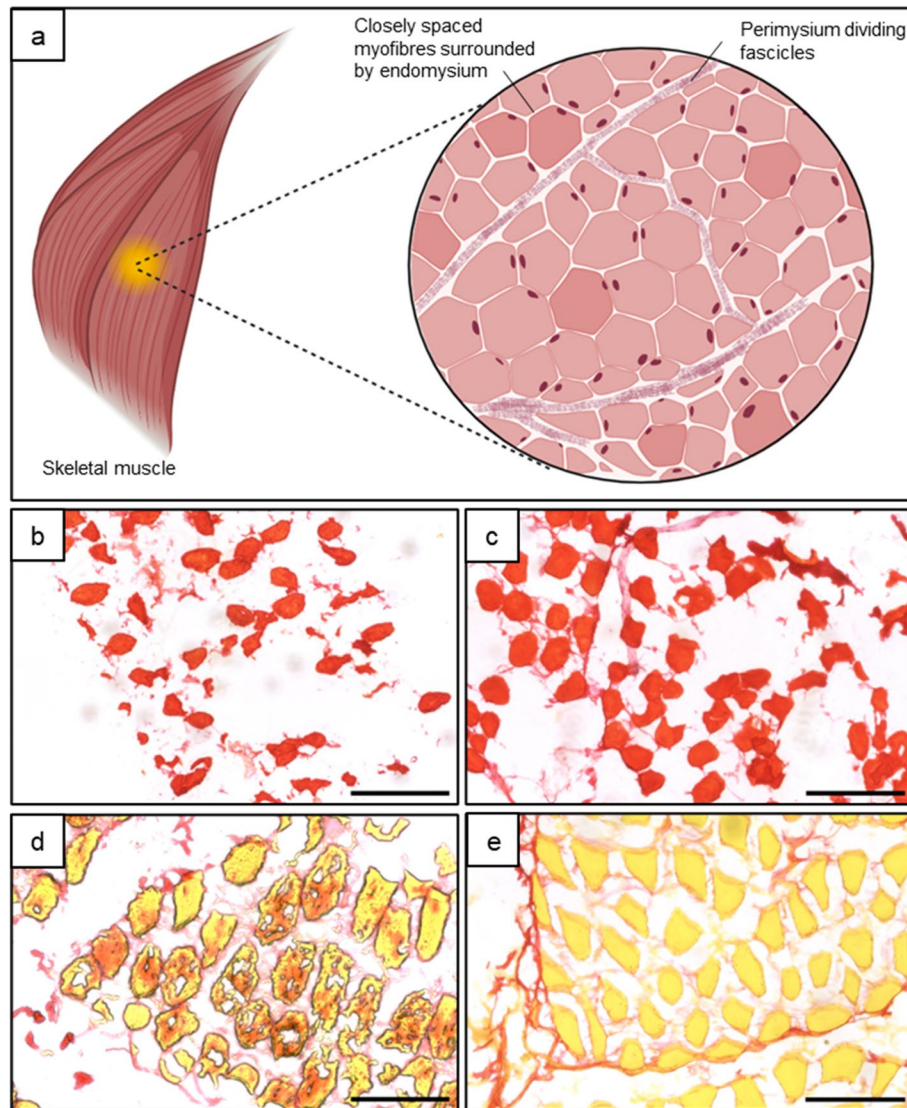


Fig. 1 Preservation methods for human skeletal muscle biopsies: schematic and PSR-stained images. **a** Schematic representation of ideal myofibre arrangement and juxtaposition; representative PSR-stained images of human skeletal muscle tissue sections preserved with various methods are shown: **b** Direct embedding in OCT without fixation; **c** Fixation with 10 % formaldehyde, followed by embedding in OCT; **d** Refreezing with LN₂, followed by embedding in OCT; **e** Fixation with 36 % formaldehyde, followed by embedding in OCT. Panel a) was created using BioRender. Scale bar = 200 μm. The images are presented to illustrate artefacts observed

vacuole-like gaps within cells, some degraded cellular structures, and no lipid staining. These features likely represent intracellular ice crystals due to inadequate freezing of tissue [20]. To assess structural changes in a myofibre resulting from the accumulation of ice crystal artefacts, fluorescence microscopy was performed using rhodamine-phalloidin to stain for actin myofilaments. Hollow regions were observed within cells stained with phalloidin, implying the presence of structures not permitting effective dye staining and light transmission; we consider these likely to be ice crystal artefacts (Fig. 2c-d).

The voids shown in the images presented in Fig. 2c is potentially where the ice crystals were located before thawing, hence the dark regions observed under confocal microscopy. These observations are important and will help to inform other investigators of potential artefact issues related to skeletal muscle processing.

The muscle biopsy sample was revealed to have been taken from a healthy male volunteer, between the age of 18 and 45, devoid of any pathological conditions. Hence, the loss of characteristic morphological features and structural integrity of the biopsy samples occurred

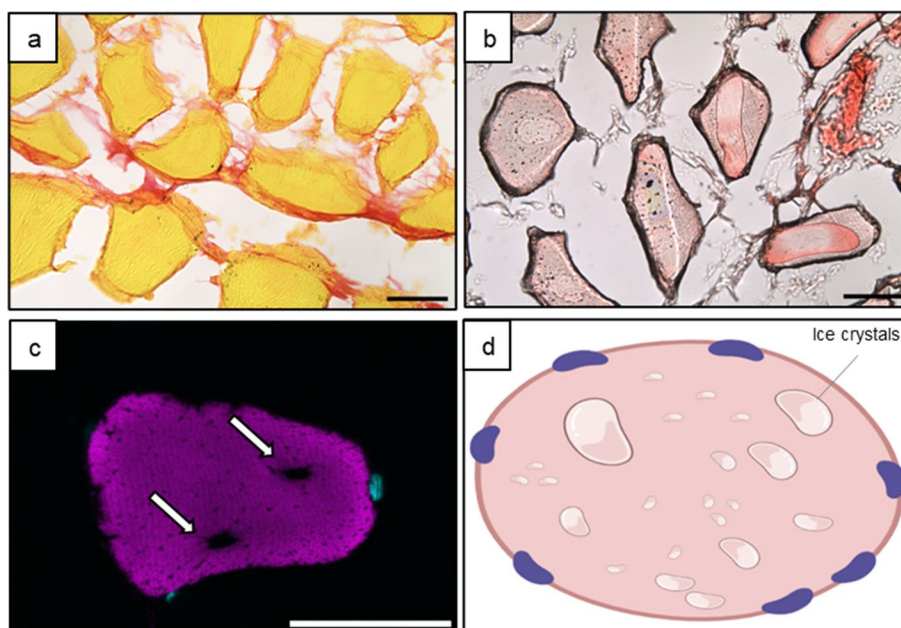


Fig. 2 Morphological analysis and schematic representation of myofibre disruption and ice crystal artefacts. **a** PSR-stained myofibres demonstrating endomysium disruption and separation of myofibres; **b** ORO-stained myofibres exhibiting the presence of intracellular vacuoles; **c** Fluorescence microscopy image stained with rhodamine-phalloidin (magenta) for actin and DAPI (cyan) for nuclei, revealing gaps within the myofibres, indicative of potential structural alterations; image has been made compatible for colourblind accessibility; **d** Schematic diagram generated using BioRender illustrating a cell with vacuoles/gaps to correlate with ice crystal artefacts. Scale bar = 50 µm

during the preservation/storage process. We recognised the importance for strict measures taken at the point when the biopsy is collected and in the way it is handled before experimentation. Based on the data presented, traditional snap-freezing and processing protocols do not preserve sample integrity, and are not recommended for light microscopy analysis.

Specimen handling – rat muscle

We decided to optimise specimen handling on rat skeletal muscle samples before embarking upon further human studies. We initially started the freezing experiments on whole muscles taken from rats, and later worked on smaller, biopsy-sized samples. At this point, fixation was abandoned as a preservation technique due to its ability to disrupt skeletal muscle structure [17, 18]. Only snap-freezing methods were employed.

Calf and thigh muscles were dissected from rat legs, frozen in LN₂ and layered on with OCT before cryosectioning. Ice crystals were observed within the muscle tissue sections (Fig. 3), an effect that has been observed in literature with the use of LN₂ as a freezing medium, arising from a slow freezing process [5]. Nitrogen has a boiling point of -196 °C. This means that to be in a liquid state, nitrogen must be at an even lower temperature. When LN₂, colder than -196 °C, encounters skeletal muscle biopsy at room temperature, it evaporates and forms a layer of vapour around the tissue. This is termed the Leidenfrost effect and hinders uniform cooling of the specimen as heat from the sample cannot dissipate rapidly enough. As a result, the overall freezing process is delayed, leading to the development of ice crystals, termed as the ‘Swiss Cheese’ effect [3, 21, 22]. This effect can be counteracted with the use of a cryoconductor, such as isopentane. In addition to ice crystals caused by

(See figure on next page.)

Fig. 3 Role of OCT in ice crystal artefact formation in skeletal muscle tissue. **a** Schematic representation illustrating the skeletal muscle structure with highlighted regions depicting the edge and belly, showcasing the differential surface-area-to-volume ratio in contact with OCT. (created in BioRender); **b-c** Sections obtained from the edge and belly regions, respectively, with a comparison between core and periphery; **d** Cross-sectional view of skeletal muscle tissue revealing a gradient in ice crystal formation from the periphery towards the core; **e** Quantitative analysis demonstrating the area occupied by ice crystals in the core and periphery of both edge and belly regions. Scale bar = 100 µm. Graphs display mean (SD); n = 4 ROIs each for core and periphery, repeated across edges and bellies of 2 biological replicates (*** = p value ≤ 0.001; ** = p value ≤ 0.01; ns = p value > 0.05; analysed using Mann Whitney U test); E: Edge; B: Belly

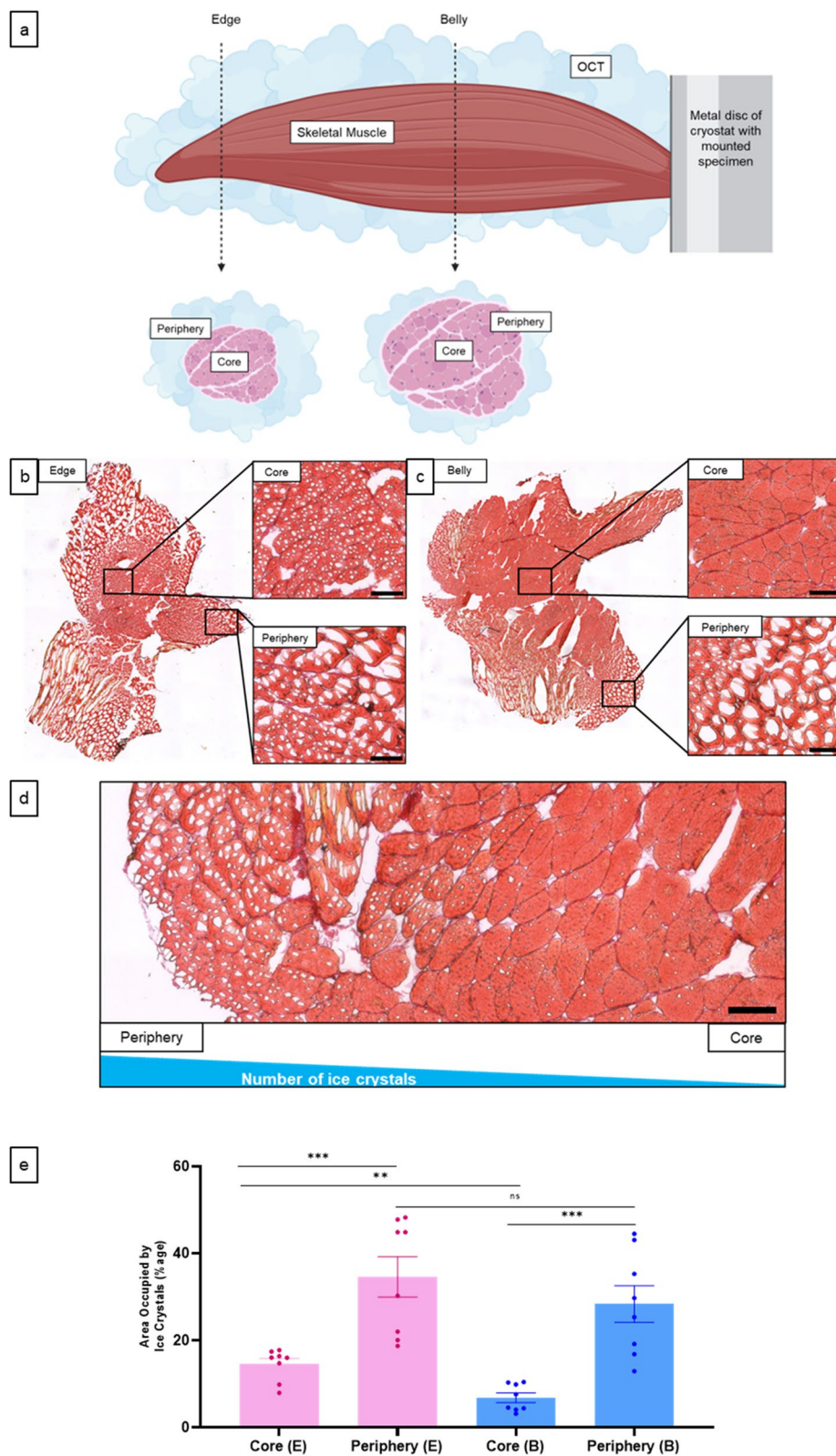


Fig. 3 (See legend on previous page.)

slow freezing, we considered the possibility of the use of OCT adding to artefact formation. We proposed that employing OCT to embed samples to allow for encapsulation of specimen right before cryosectioning contributes to freezing artefacts visualised in our samples. Previous studies in the literature advise against the use of OCT for skeletal muscles as they have a high endogenous water content, and OCT adds moisture to the tissue [5, 6, 23]. Certain skeletal muscles types have tapering edges and thicker bellies (see Fig. 3a), such as the bipennate and fusiform muscles in the lower limb [20]. The surface area-to-volume ratio varies along these muscle samples, potentially leading to differences in OCT penetration with concomitant effects on tissue morphology or artefact formation. There is greater contact of the tissue with OCT at the edges due to their tapering nature, and a higher surface-area-to-volume ratio. Moreover, within the same section, comparing the core and periphery of the tissue provides us with information on the potential effect of OCT, as the periphery is in direct contact with the compound (Fig. 3a). Representative images of PSR-stained tissue sections taken from both the edge and belly of the muscle are shown in Fig. 3b and c respectively. A greater number of ice crystals can be visualised in the core region of the edge as compared to the belly. At the periphery, large ice crystals are observed in sections taken from both the edge and belly of the muscle, representing coalescing crystals. Even within the same section, the number and size of ice crystals decreases moving from the periphery to core (Fig. 3d). These changes were seen when we quantified the percentage area occupied by ice crystals for the core and periphery in sections from the edge and belly (Supplementary Table 5 & Fig. 3e). At this point, we concluded that the use of OCT contributes to, and worsens, the formation of ice crystal artefacts within the skeletal muscle tissue sections, and all future cryosectioning procedures were performed without embedding in OCT.

Scaling down the sample size

The whole muscle samples dissected from rats did not truly mimic human muscle biopsies, owing to the difference in size. The core biopsies for human studies are up to 1 cm length, 14 to 18 gauge (diameter of 1.6 to 1.0 mm) [24]. Therefore, there was an unmet need to develop freezing protocols on specimens with sizes comparable to human needle biopsy.

Figure 4a shows the steps followed to obtain rat skeletal muscles 'biopsies'. The leg muscles were excised in the BPU and transported in a saline-moistened gauze to our laboratory with the freezing setup in place. The saline-moistened gauze was employed to prevent the drying up of tissues. Using scissors and a scalpel, the muscles were

dissected out and cut into smaller biopsy-sized pieces and used for subsequent freezing protocols. We developed an experimental protocol to snap freeze rat skeletal muscle 'biopsies' in LN₂ and isopentane pre-cooled with LN₂. For each, we either directly immersed the specimen in the freezing medium, placed the specimen in a histocassette before immersion or dipped the specimen in OCT to provide a sufficient encapsulating layer, followed by immersion in freezing media (Fig. 4b). The use of OCT was abandoned before cryosectioning (see above), but an OCT base was allowed for attachment of the sample to the metal holder disc of the cryostat (Fig. 4c). A clear distinction can be observed between samples cryosectioned with and without OCT layering (Fig. 4d), further reaffirming the deleterious effects reported above.

Tissue sections were stained with PSR to visualise details of myofibre arrangement in fascicles as well as the structural integrity of the endomysium/perimysium, comparing the core and periphery of each section. H&E staining was conducted to further reaffirm myofibre and myonuclei positioning, as well as to visualise ice crystals within the cytoplasm that can provide evidence of cellular alterations and structural anomalies induced by freezing protocols.

Figure 5 demonstrates that for the use of smaller pieces of skeletal muscles, e.g. biopsies, LN₂ can provide preservation of the structure, with and without histocassettes, in the core of the specimen. Ice crystals persist at the periphery. With the sample dipped in OCT, followed by subsequent LN₂ immersion, crystals are observed in both the core and periphery. Samples immersed in pre-cooled isopentane, with or without the OCT dip, presented a picture similar to that of direct immersion in LN₂, with artefacts present only at the periphery of the sample. Placing the specimen in a histocassette prior to snap-freezing with pre-cooled isopentane minimised ice crystal formation in both the core and the periphery of the specimen.

Assessing myofibrillar organisation and fluorescent staining in fixed sections

For assessment of myofibrillar morphology, as well as organisation of cellular organelles, we stained for myonuclei, actin myofilaments, and skeletal muscle mitochondria, to be visualised using fluorescence microscopy. The fluorescence microscopy images obtained for core regions for sections frozen in the six different cryopreservation methods are shown in Fig. 6. The myofibrillar orientation and branched distribution of mitochondria are intact in all specimens cryopreserved in LN₂ (direct, dipped in OCT, and in a histocassette) as well as after direct immersion in pre-cooled isopentane.

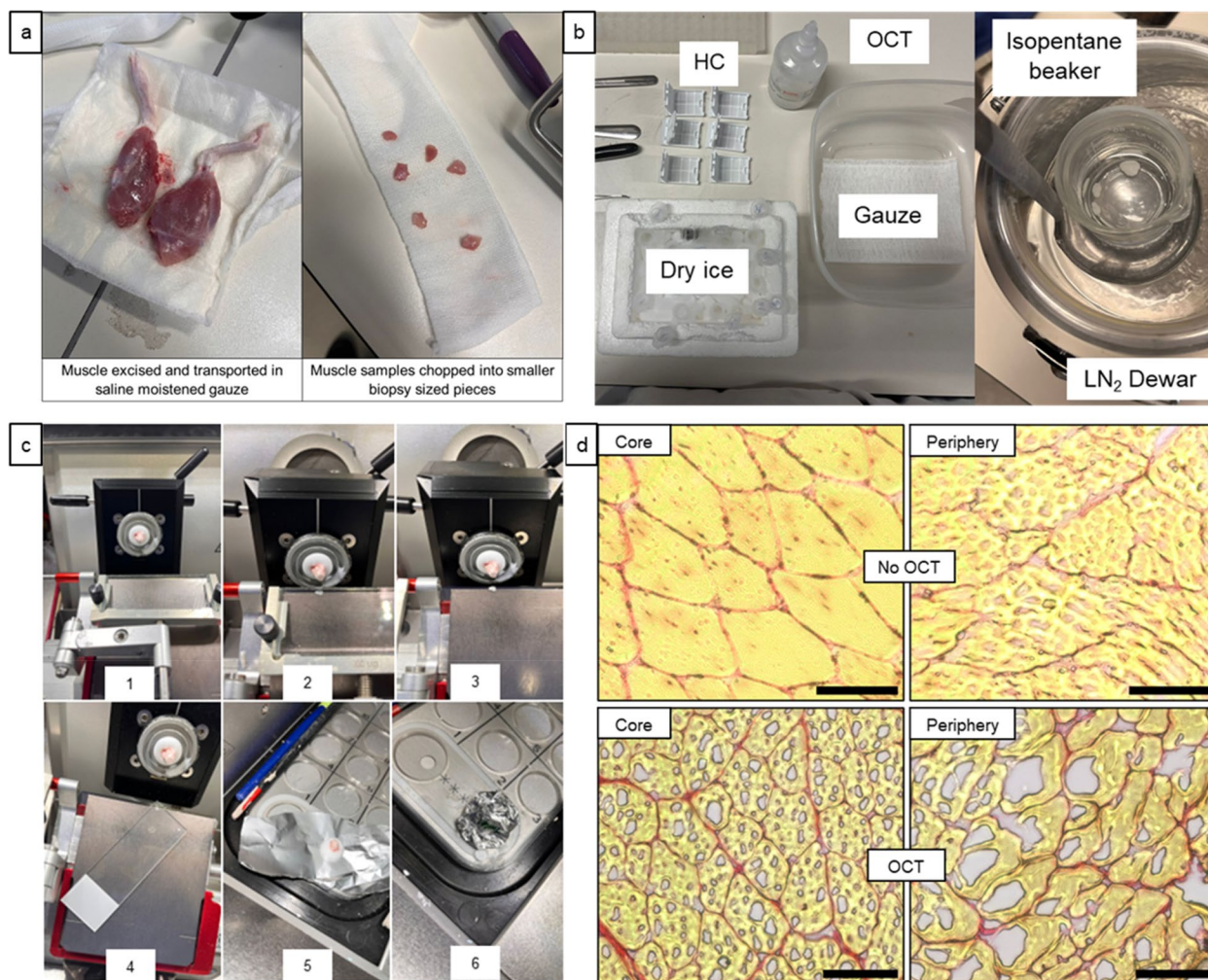


Fig. 4 Sample collection and cryosectioning procedure for rat skeletal muscle tissue freezing. **a** Visualization of the process of cutting small biopsy-sized pieces of muscle from rat legs; **b** Experimental setup utilised for freezing including a dewar for LN₂ and a beaker mounted on a ladle for isopentane. Histicassettes (HC) are shown. The gauze was slightly moistened with saline to transport the muscle sample from the dissected rat to the freezing setup. Dry ice was used to pre-cool 1.5 mL tubes and forceps; **c** Step-by-step procedure of mounting frozen muscle onto OCT base, attachment of metallic holder disc within a cryostat (1), sectioning tissue (2), carefully lifting the anti-roll plate (3), transferring section to SuperFrost slide (4), placing leftover sample with OCT base in pre-cooled aluminium foil (5), and wrapping sample with foil before storage in -80 °C; **d** Representative PSR-stained sections of skeletal muscle tissue, with and without OCT, highlighting differences in ice crystal formation between the core and periphery. Scale bar = 20 μm

As for specimens frozen in pre-cooled isopentane with OCT dip, disruption of myofibrils is observed, with large gaps within the myofibrils representing ice crystals. The mitochondrial distribution with respect to myofibrils remains intact. Despite the presences of ice crystal artefacts and the consequent alteration in myofibrillar architecture, the mitochondrial network remains distributed between the myofibrils. Gaps within myofibrils are filled with the mitochondria. Therefore, an additional advantage of staining the mitochondria is the ability to differentiate between actual anatomical architecture and gaps formed by ice crystals (which will not be stained with

mitochondrial dye). Specimens frozen in pre-cooled isopentane after placement in a histicassette show complete preservation of myofibre morphology and an absence of gaps arising from ice crystal artefacts.

The peripheral regions of sections obtained from each of the cryopreservation procedures show large ice crystal gaps, with some cases of saturation of the fluorescent signal. Myofibrillar disruption is also observed, and some sections did not stain for the mitochondria at the periphery at all. In keeping with our results for the core regions, the periphery of specimens frozen with pre-cooled isopentane following placement in a histicassette showed

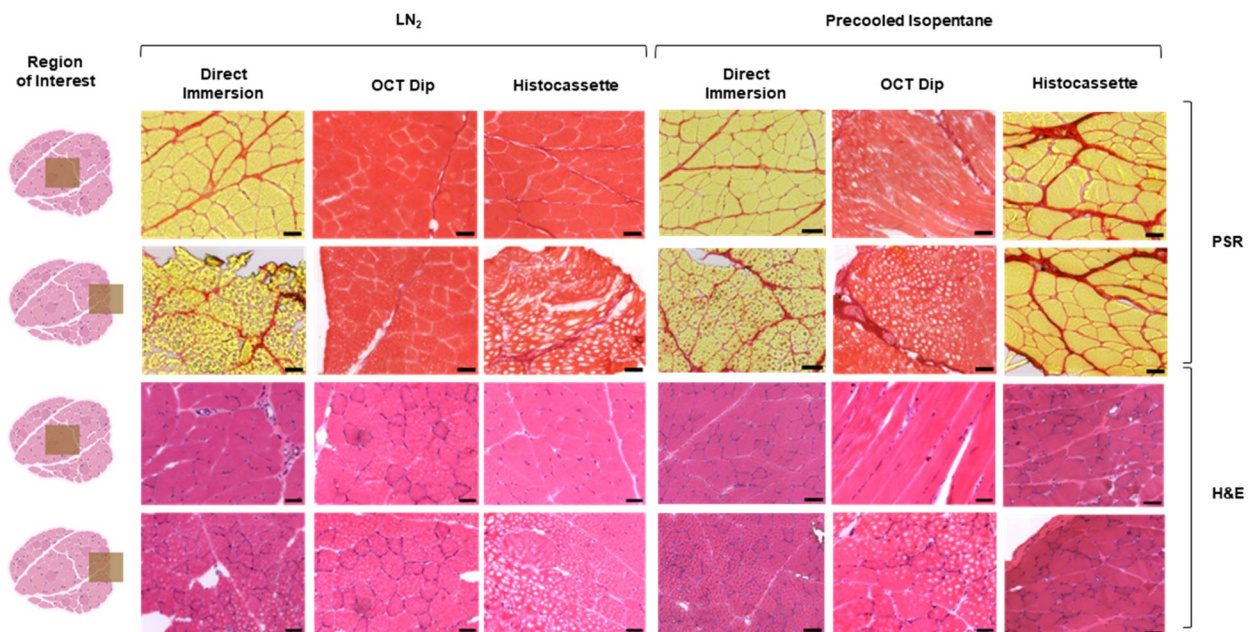


Fig. 5 Comparison of skeletal muscle tissue freezing methods using PSR and H&E staining. Representative PSR and H&E images provide visual comparisons of tissue morphology and ice crystal formation between core and periphery regions under various freezing conditions, utilising LN₂ and pre-cooled isopentane, as labelled. Scale bar = 50 μ m

intact architecture, no ice crystals, and adequate staining of tissue.

Complete preservation of both the core and periphery of tissue sections is critical due to the limited tissue volume obtained with needle biopsies. Given the small size of these biopsy samples, any ice crystal artefacts can significantly impact the integrity and representativeness of the entire specimen. Our study demonstrates that the isopentane/histocassette combination uniquely provides artefact-free preservation across the entire tissue section, making it the most effective method for cryopreservation of skeletal muscle biopsies (Fig. 7). This method ensures that both central and peripheral regions of the tissue are maintained without structural disruption, thereby preserving the biopsy's diagnostic and analytical value.

Mitochondrial analysis workflow

The next step in our study was to optimise the analytical procedures. The mitochondrial workflow we created using currently available Fiji functions and plugins, e.g. background subtraction, Trainable Weka Segmentation, binarisation, skeletonisation and MiNA (described below), can be employed for mitochondrial quantification analysis of entire cells or for multiple ROIs within the same cell. Moreover, the workflow can be modified to generate a map of the mitochondrial network, with the mitochondria and branches separately highlighted,

to allow for localisation of targets of interest on confocal imaging.

Figure 8a shows differences in size, capillary density, myoglobin concentration and mitochondrial size and number among the three myofibre types. Type I fibres are the smallest in diameter, have the highest concentration of myoglobin (hence the darker colour), have the richest capillary network distribution, and contain larger and more abundant mitochondria. Type IIb myofibres show a decreased myoglobin concentration, capillary density as well as mitochondrial size and number, whereas cell diameter increases [25]. Figures 8b and c show how the mitochondrial network is distributed within the cell architecture in a transverse and longitudinal section. The density of mitochondrial content varies with different fibre types and, as observed in the fluorescence microscopy images in Fig. 8c, type I myofibres, smaller in size, stain heavily for mitochondria, and the larger type II myofibres show a weaker mitochondrial signal. This can be helpful in differentiating fibre types within the tissue Sect. [25, 26].

For our analysis, we employed transverse cell sections (Fig. 8d), because highly magnified images are necessary for adequate distinction of the mitochondrial network, and longitudinal sections do not allow entire cells to be captured at the required zoom level.

The mitochondrial analysis workflow is presented in Fig. 9. For representative analysis, we used an image

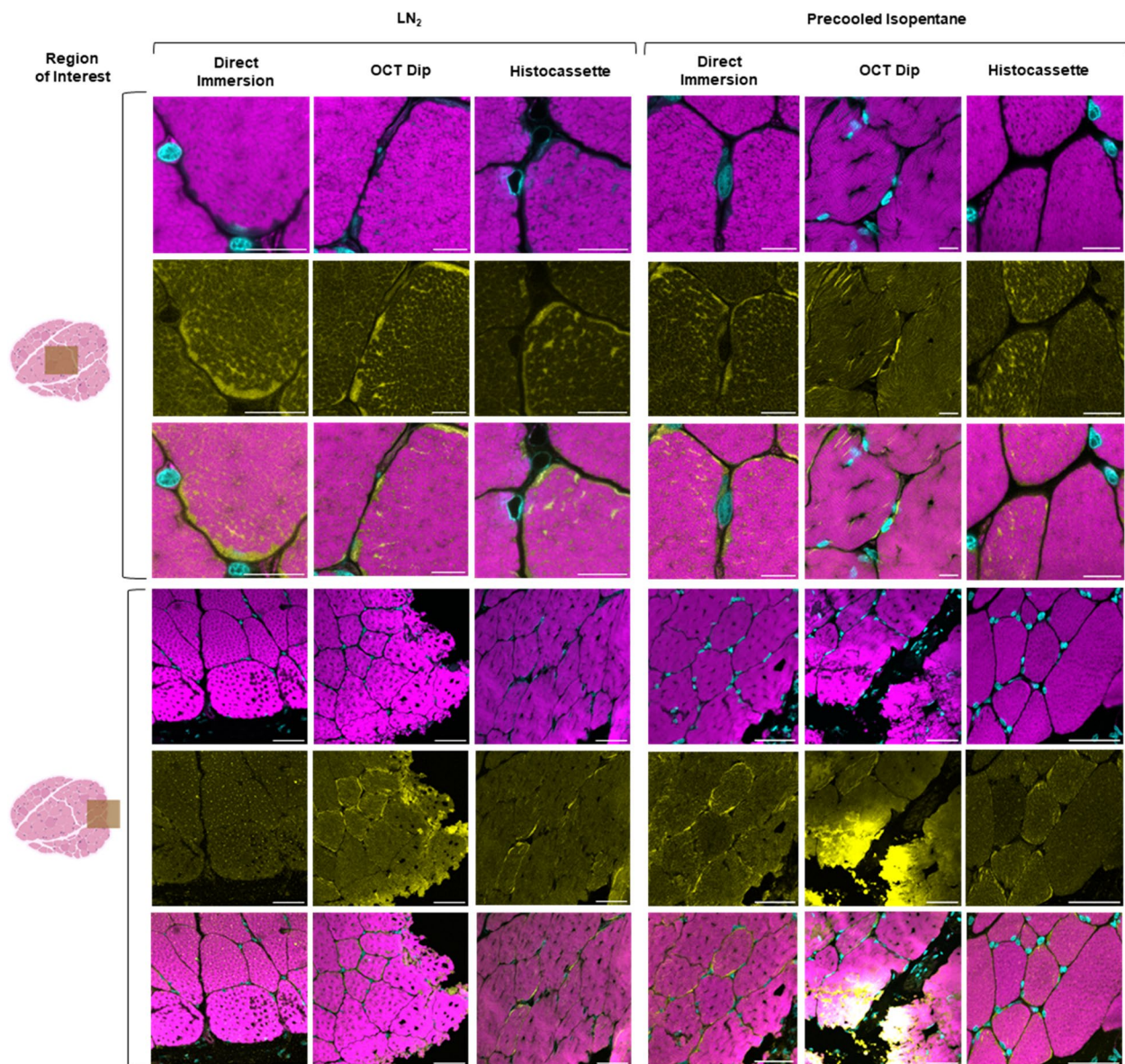


Fig. 6 Assessment of structural integrity in core and peripheral regions of skeletal muscle tissue sections using fluorescence staining. Representative fluorescence microscopy images of core and periphery regions of skeletal muscle tissue sections stained with MitoView (yellow), phalloidin (magenta), and DAPI (cyan) to evaluate tissue morphology following freezing with six different methods as labelled. Scale bar = periphery 50 μ m; core 10 μ m. Images have been made compatible for colourblind accessibility

showing both type I and II myofibres. This allowed us to generate a workflow that could be employed for quantification analysis of both fibre types – as both will be found in skeletal tissue sections. We analysed both fibre types separately as concurrent analysis could potentially limit the detection of the weaker mitochondrial signal in type II fibres. In skeletal muscle tissue sections, cells are in tight juxtaposition with each other, mostly with type I and II fibres adjacent to each other. To isolate the cell of interest and ensure our analysis is

conducted on only one cell, we utilised the polygonal selection tool.

The high background noise in tissue sections stained with MitoView Green necessitated background subtraction as a pre-processing step. This enhanced the signal-to-noise ratio. For the next part of our workflow, we adopted the use of Trainable Weka Segmentation plugin in Fiji which employs a machine-learning algorithm to segment images based on their pixel intensity [27]. This plugin can be trained to distinguish between actual signal

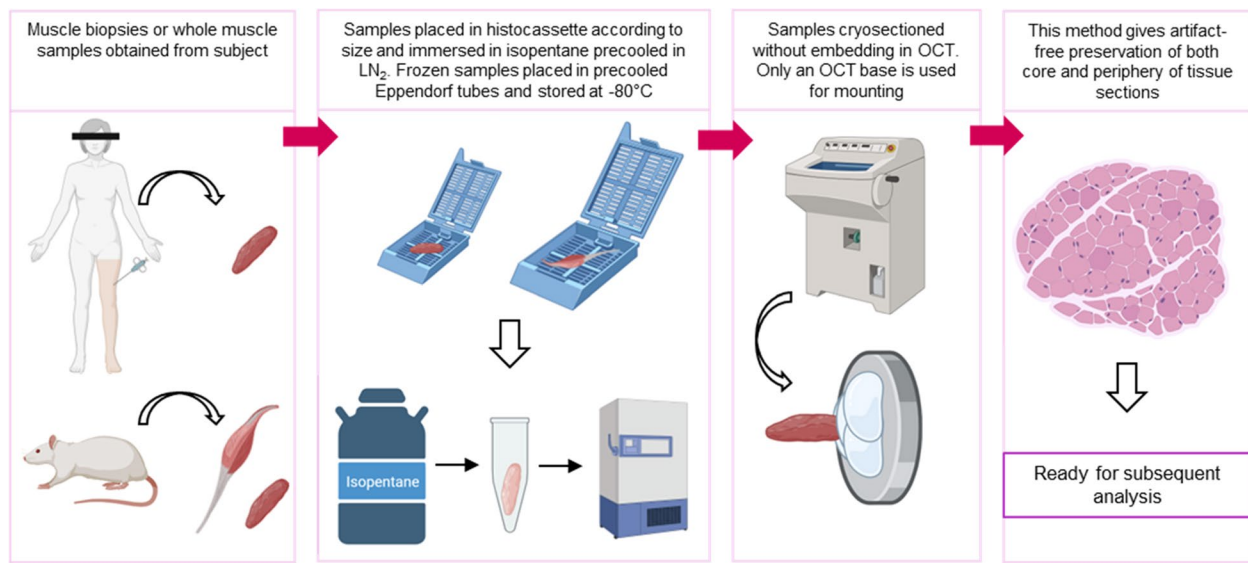


Fig. 7 Optimal Handling Conditions for Skeletal Muscle Specimens. This figure illustrates our recommended protocol for cryopreservation of skeletal muscle tissue samples to ensure optimal preservation for subsequent analyses. Diagram created using BioRender

and noise, simply by adding different traces under those classes. We utilised the freehand selection tool for this purpose. Once traces for each class had been drawn, the plugin was then trained resulting in a segmented image overlaid on the original input (Supplementary Fig. 1). Probability maps were generated, which illustrated the probability of each pixel being correctly assigned to one of the classes. The probability map for our signal, termed the 'signal mask', was then duplicated for subsequent analysis. The signal mask should completely overlay the original mitochondrial signal, and, for our image analysis, this was confirmed via subtraction of the mask from the original confocal image. We noted that the signal mask contained spurious low-intensity signal around the mitochondrial signal structure, likely originating from the low-probability assignments in our analysis, which hindered accurate subsequent analysis (Supplementary Fig. 2). The optimal method to mitigate this spurious signal was to re-process the signal mask using a second round of Trainable Weka Segmentation. The final signal mask generated was then duplicated and binarised (Process Binary Make Binary). To confirm that the mitochondrial network was accurately captured, we skeletonised the binarised image (Process Binary Skeletonise). Skeleton subtraction from the original image was performed as above for confirmation. The final binarised signal mask was then analysed using the MiNA plugin to obtain various mitochondrial network parameters.

The trained classifier and trace data can be saved and used again for application on different images. Figure 10 shows the same classifier and trace data being employed

for the type II myofibre in the original image (after being isolated with a polygonal selection tool). Once the classifier and data were loaded onto the Weka plugin window, the overlaid image was assessed to ensure that signal and noise were adequately differentiated. Otherwise, more traces can be added, and the plugin can be trained again to incorporate this information into the loaded data and classifier. We have made the training parameters openly available for other users to use with our example mitochondrial images.

As previously explained, the workflows in the literature are adapted to cells, and do not account for the noise in skeletal muscle tissue sections observed with dyes such as MitoView Green [11, 12]. This leads to inadequate thresholding and loss of signal for subsequent steps. Figure 11 demonstrates how our workflow employing Trainable Weka Segmentation can lead to appropriate thresholding, capturing mitochondrial signal in both type I and II fibre types, as compared to existing workflows.

To further validate our mitochondrial analysis workflow, multiple ROIs were created for both type I and II myofibres, and the MiNA plugin was then employed (with no pre-processing and Otsu adaptive thresholding). This permitted various quantitative parameters to be obtained. An understanding of the nomenclature adopted by the MiNA plugin is essential here.

The skeleton formed by the MiNA plugin broadly consists of two different mitochondrial features: individuals (structures without junctions) and networks (structures with junctions). Single pixels within the skeleton (puncta), two or more pixels without branching (a rod),

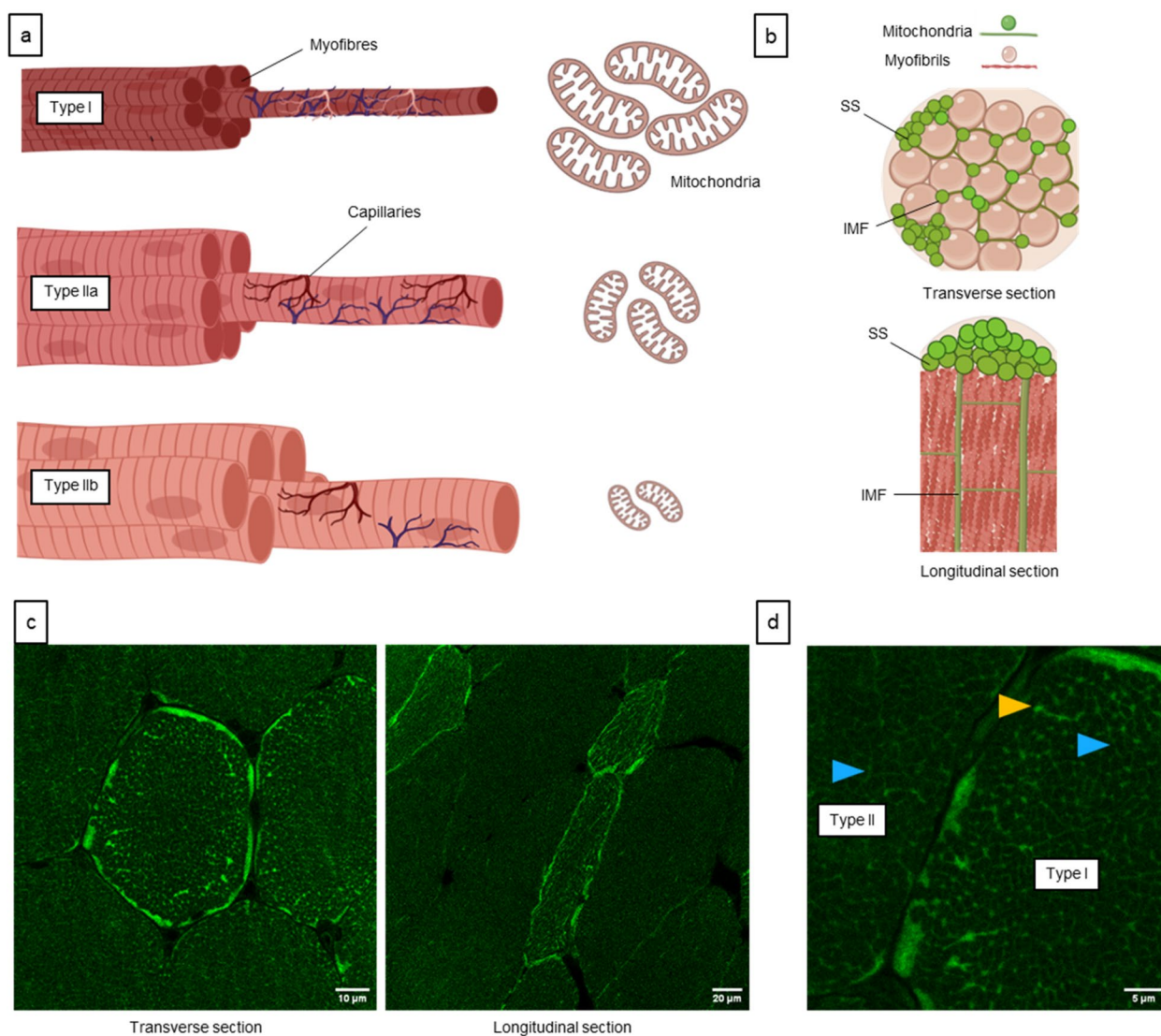


Fig. 8 Mitochondrial Morphology in Skeletal Muscle Tissue. **a** Schematic representation of different types of myofibres, illustrating variations in myoglobin concentration, capillary density, diameter, and mitochondrial content; **b** Schematic illustration demonstrating distribution of mitochondria in transverse and longitudinal sections of skeletal muscle, showcasing their characteristic arrangement around the myofibrils. **c** Fluorescence microscopy images demonstrating the distribution of mitochondria in transverse and longitudinal sections of skeletal muscle stained with MitoView Green **(d)** Close-up of skeletal muscle tissue section stained with MitoView Green, showing both type I and II myofibres, with brightly (orange arrow) and dimly (blue arrows) stained mitochondria. SS: subsarcolemmal mitochondria; IMF: intermyofibrillar mitochondria

and round structures which are potentially smaller networks – all are considered as individuals. At least three branches connected at a junction are considered a network (Fig. 12) [28].

The image or ROI may contain multiple mitochondrial structures. A structure can be either an individual or a network. Using the MiNA plugin, various quantitative parameters can be obtained: 1) The ‘mean branch length’—depicts the average length of all individuals/branches within the skeleton in the ROI. 2) The ‘mean summed branch length’ – depicts the average length of

branches per mitochondrial structure, reflecting the size and extent of an individual mitochondrial network. 3) The ‘mean network branches’ – depicts the average number of branches for each independent mitochondrial network in the ROI, reflecting the complexity of each mitochondrial structure. This gives an idea of how branched or interconnected each mitochondrial network tends to be. 4) The mitochondrial footprint is the total area occupied by the mitochondrial signal in the image or ROI. This gives an idea of mitochondrial content within the ROI and reveals why isolating cells with the polygonal

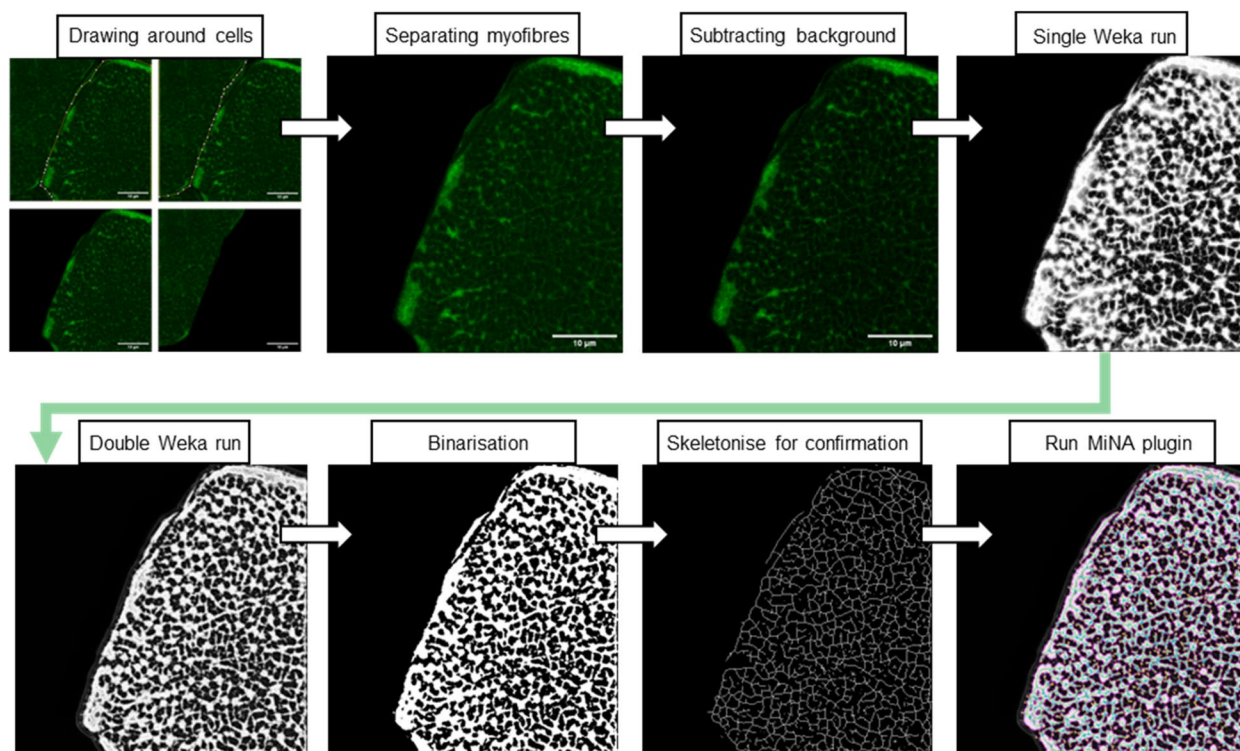


Fig. 9 Workflow for mitochondrial analysis in type I myofibres using Trainable Weka Segmentation in Fiji. Outline individual cells to focus on one particular myofibre type, remove background noise to enhance clarity of mitochondrial signal, apply the Trainable Weka Segmentation plugin to discern mitochondrial network, run through Weka again to obtain clearer signal mask, convert the signal mask to binarised image, use skeletonise function to confirm the map of the mitochondrial network, run the binarised signal mask through the MiNA plugin to obtain quantitative parameters

tool, or using ROIs with a known fixed area is essential to ensure accurate comparisons across images/cells. Supplementary Table 6 and Fig. 13 show a comparison between ROIs from type I and type II myofibres from our previous analyses. The mitochondrial footprint and mean branch length in type I myofibres are significantly higher than those in type II myofibres, whereas the mean summed branch length and mean network branches show no significant difference between the two myofibre types. Assessment of such parameters provides insight into changes in mitochondria that may occur as an impact of ageing on muscle tissues, pathology of neuromuscular disorders, and adaptations from exercise training [29–32].

A practical guide to mapping mitochondrial networks

We next considered how our approach could be modified to generate a map of the mitochondrial network to allow for spatial localisation of targets of interest in relation to the mitochondria imaged using confocal imaging. Figure 14 demonstrates the textual (14a) and visual (14b) workflow employed for this purpose.

Localisation of target of interest – challenges with antibody penetration

We conducted immunofluorescence staining to evaluate antibody-based protein detection within skeletal muscle tissue sections. In this context, we immunostained the VDAC, a well-established mitochondrial marker that is present on the outer mitochondrial membrane. Samples were counterstained with MitoView Green and DAPI to assess the spatial relationship of VDAC with respect to the mitochondria and nucleus in our skeletal muscle tissue sections. Interestingly, while the mitochondrial and nuclear dyes were uniformly distributed throughout the entire tissue section, VDAC immunostaining was limited to certain depths of view.

To assess the depth of penetration of the antibody, we performed 3D confocal imaging, with subsequent utilisation of *temporal hyperstack* function in Fiji. This plugin enabled us to visualise the fluorescence signal along the z-axis by colour-coding signal intensity according to the extent of penetration depth by the antibody (Fig. 15). The colour-coded image projection revealed that the VDAC signal was predominantly localised to the apical layer of the section, in contrast

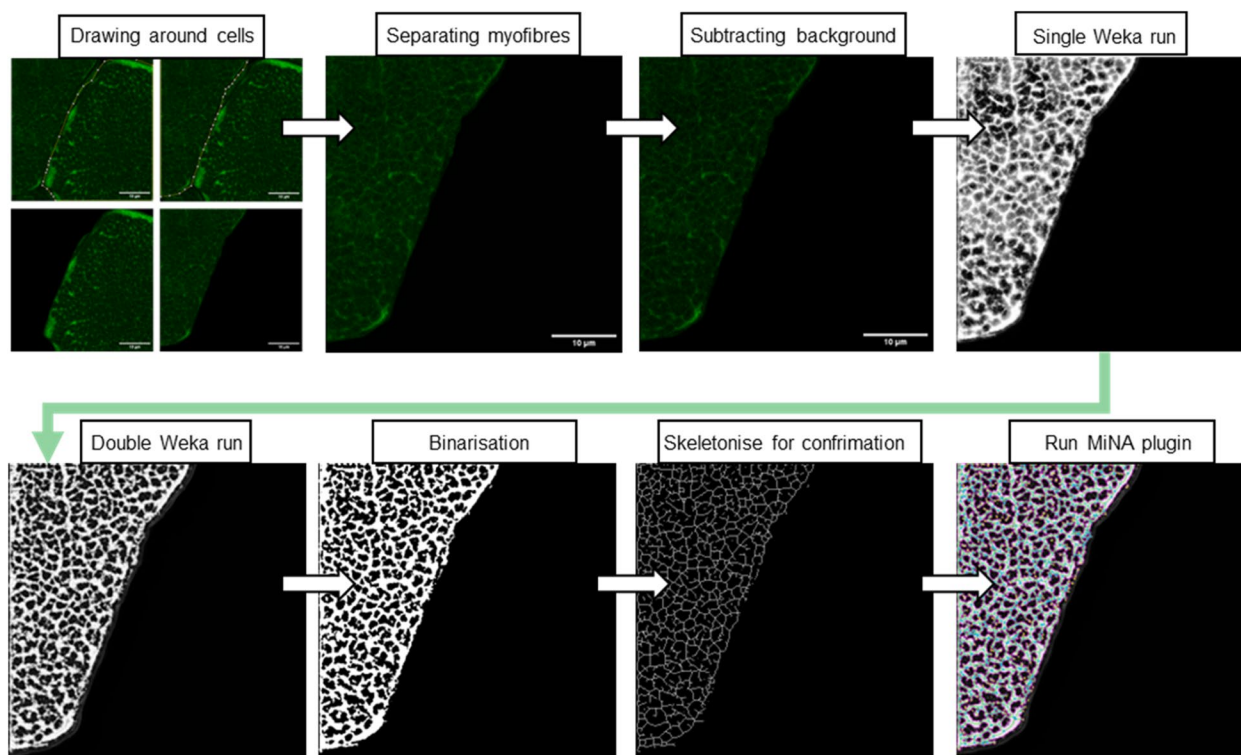


Fig. 10 Workflow for mitochondrial analysis in type II myofibres using Trainable Weka Segmentation in Fiji. Outline individual cells to focus on one particular myofibre type, remove background noise to enhance clarity of mitochondrial signal, apply the Trainable Weka Segmentation plugin to discern mitochondrial network, run through Weka again to obtain clearer signal mask, convert the signal mask to binarised image, use skeletonise function to confirm the map of the mitochondrial network, run the binarised signal mask through the MiNA plugin to obtain quantitative parameters

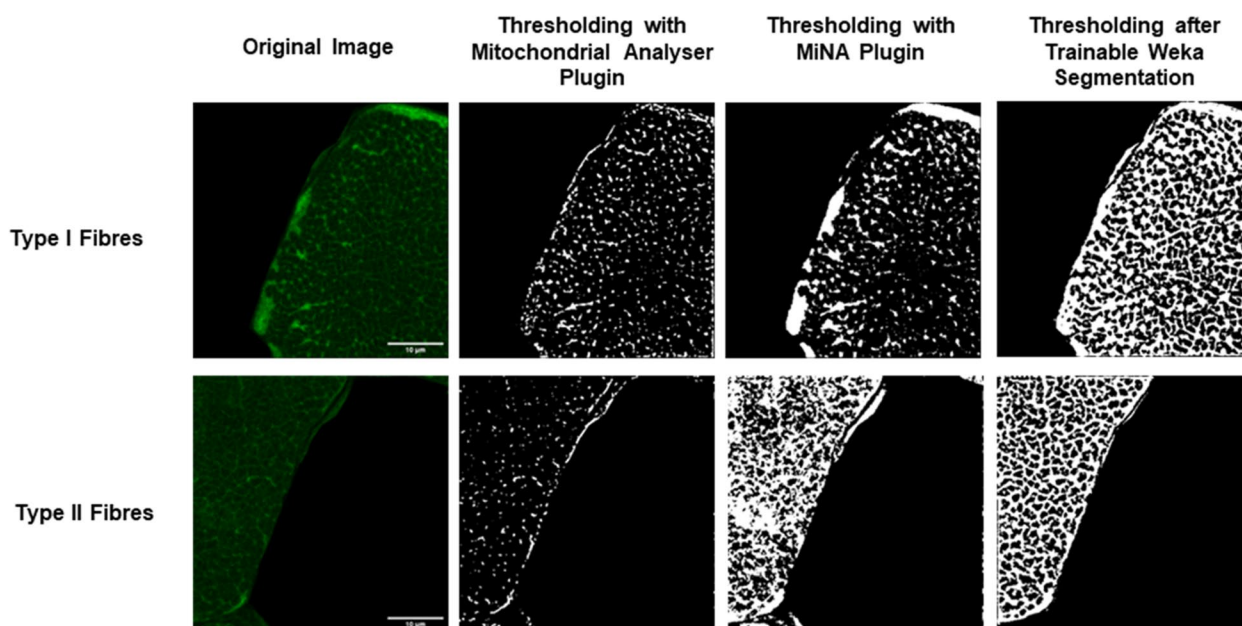


Fig. 11 Thresholding type I and II myofibres using Mitochondrial Analyser, MiNA and Trainable Weka Segmentation plugins. Employing the Weka plugin produces a signal mask mapping the mitochondrial network distinguished clearly from the background despite the low signal-to-noise ratio

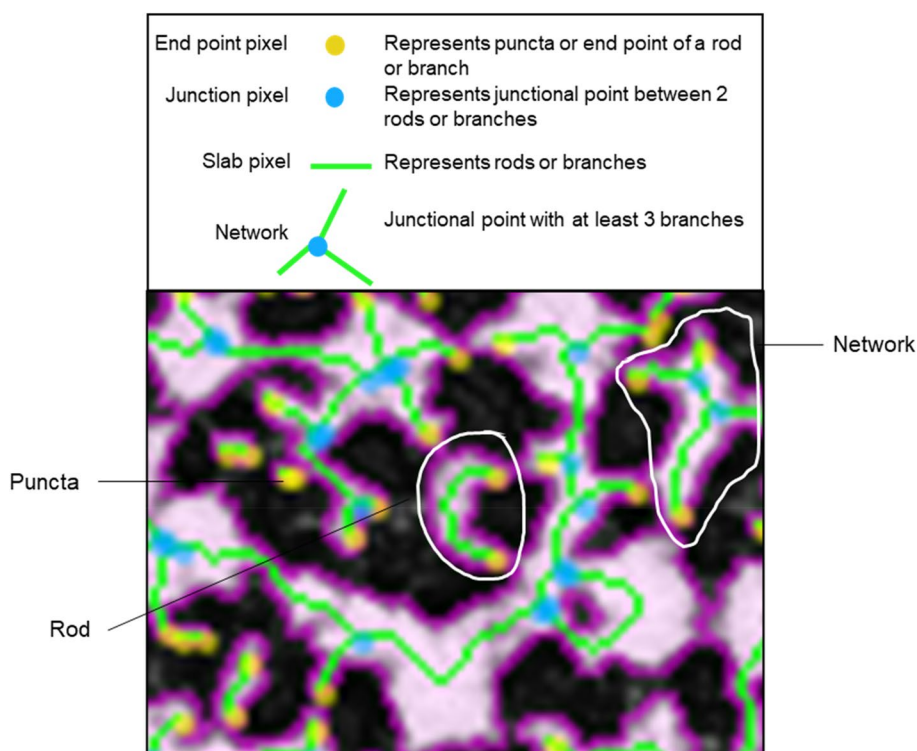


Fig. 12 Representation of nomenclature employed by MiNA plugin on skeleton generated by our workflow. A mitochondrial structure in the skeleton created as part of MiNA analysis may be an individual (puncta or rod), or a network (a junctional node with at least 3 branches)

to MitoView Green and DAPI, which permeated through the entire tissue depth.

To improve antibody penetration, we decided to permeabilise our tissue sample with 0.5% (v/v) Triton X-100 in PBS instead of 0.25% Triton X-100 [33]. However, the antibody penetration was similar to what was observed with 0.25% Triton X-100 permeabilisation. Next, we substituted phosphate-buffered Triton X-100 (PBT) in place of PBS for all rinsing steps, also replacing 0.1% BSA for antibody incubating steps. PBT consisted of PBS with 0.01% (v/v) Triton X-100 and 0.5% (w/v) BSA and has been employed in the literature for immunohistochemical experiments to enhance antibody penetration into the tissue and reduce non-specific background staining [34]. We observed patches of tissue with deeper antibody penetration than before and this hints towards some extent of success with the use of PBT. However, further optimisation is required to get the VDAC antibody in the same planes as the dyes. These differences in antibody penetration as opposed to dyes are presented in Fig. 15 and Supplementary Fig. 3.

Discussion

Careful preservation of the morphology of clinical biopsy samples is an essential factor for tissue analysis. Given the particular difficulties in handling skeletal muscle biopsies,

with their unique multinucleate cellular morphology, the first goal of this study was to explore and refine preservation methods for skeletal muscle tissues, while assessing structural integrity using histological and immunohistochemical staining methods.

The initial phase of our study involved handling of human needle biopsies. Variation in freezing conditions can lead to disruption of cells, organelles and connective tissue. Therefore, our first objective was to examine these biopsies in detail. In our study, immersion of human needle biopsies that were originally frozen in LN₂ and stored at -80 °C caused the development of ice crystal artefacts. Fixing samples in formaldehyde or embedding in OCT, both at room temperature, resulted in the thawing of skeletal muscle samples and consequent refreezing before cryosectioning, causing further architectural changes. This effectively created a freeze-thaw cycle, leading to damage to tissue architecture. This damage presented as cellular and connective tissue streaks with no identifiable myofibres. Increasing concentrations of formaldehyde to levels much higher than the standard recommendations preserved the myofibres, as the fixating power of formaldehyde ultimately overcomes the degenerating capacity of freeze-thaw. However, even with such high fixative concentrations, we still observed structural alterations within the tissue, with widely spaced cells and disrupted

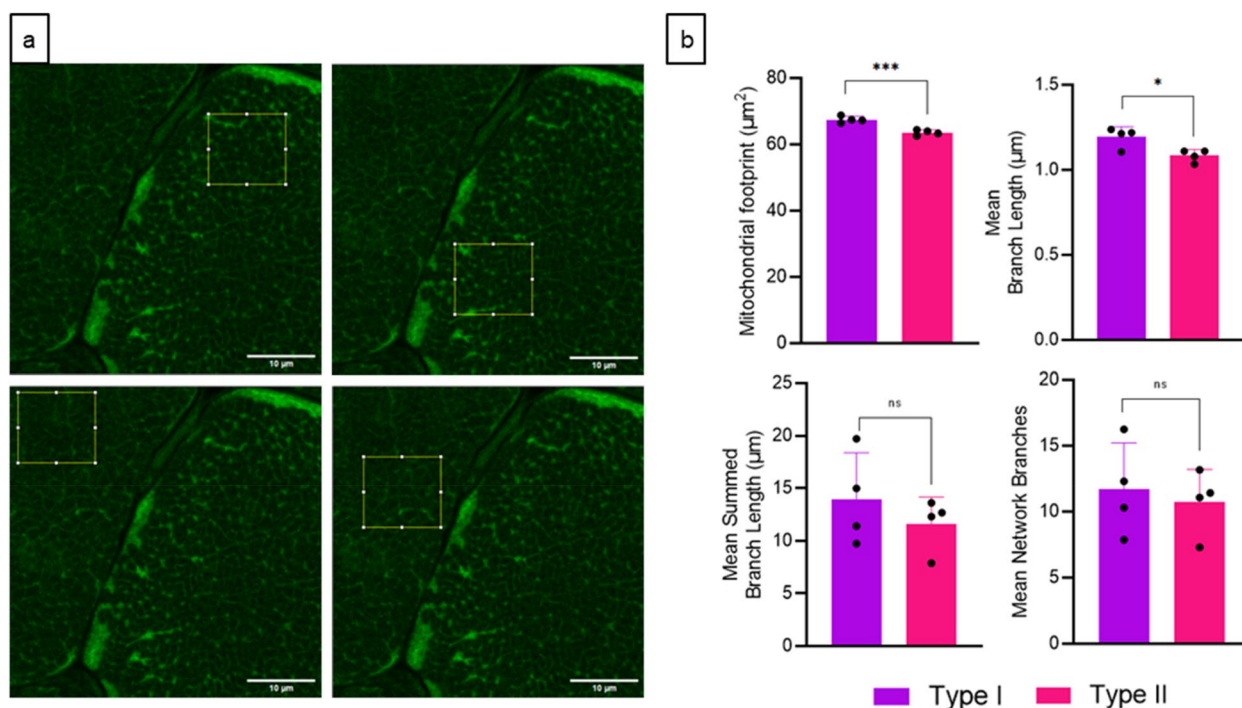


Fig. 13 Mitochondrial analysis in adjacent type I and type II myofibres. **a** Representative images of ROIs drawn in adjacent type I and type II myofibres. ROIs were selected for mitochondrial analysis using the MiNA plugin following our workflow. **b** Graphical representation of four different mitochondrial parameters: footprint, mean branch length, summed mean branch length, and mean network branches. Graphs display mean (SD); $n=4$ ROIs per fibre type; ***= p value ≤ 0.001 ; *= p value $0.01 - 0.05$; ns= p value > 0.05 ; analysed unpaired t test

endomysium/perimysium. We also observed the formation of ice crystals. This is due to the high endogenous water content of skeletal muscles, which was not prevented using elevated concentrations of formaldehyde.

The next phase of our study used rat skeletal muscle to enable experimental optimisation. This approach allowed us to compare various cryopreservation techniques, while affording greater control and flexibility. The initial decision to work on whole muscle samples, much larger than needle biopsies, provided an opportunity to develop a deeper understanding of the localisation of ice crystals and what conditions might facilitate their development. The observation of differential ice crystal distribution between sections obtained from the edge and belly of the whole muscle sample, as well as differences in the area occupied by crystals between core and periphery within the same section (Fig. 3b-e), suggested against the use of OCT. The employment of OCT has been advocated in various tissue repository guidelines for maximum preservation of cell morphology and structure [17, 35, 36]. However, the presence and extent of ice crystals in different regions of the tissue suggested that OCT may contribute to uneven crystal distribution. Muscle biopsy handling studies recommend against the use of OCT before cryosectioning since OCT can add moisture

of its own to the tissue sample, as well as compromise adequate freezing [5]. Only an OCT base is required to allow the tissue specimen to stick to the metal holder of the cryostat [23]. Here, we have demonstrated the underlying effect OCT has on sample integrity (Figs. 3b-e and 4d). We therefore decided to discontinue the use of OCT in our experimental workflow and opted to directly freeze samples without OCT embedment. The challenges related to ice formation, growth, and recrystallization during cryopreservation, as discussed by Chang and Zhou (2021), further support our decision, as cryoprotective agents like those in OCT cannot fully prevent ice damage, particularly in water-rich tissues such as skeletal muscle [37].

Moreover, the Swiss Cheese effect was observed in rat whole muscle samples cryopreserved in LN₂, suggesting nonuniform and slow cooling of tissue [6, 22]. When LN₂ encounters the warmer surface of the tissue, it forms an insulating layer of vapours encapsulating the specimen, preventing direct contact with LN₂ and hence, slower and uneven freezing—the Leidenfrost effect [38]. To overcome this, the use of isopentane pre-cooled in LN₂ has been advocated [39]. Isopentane has a melting point of -160 °C, which means that when cooled by LN₂, it moves from a liquid state to a solid state, eliminating the

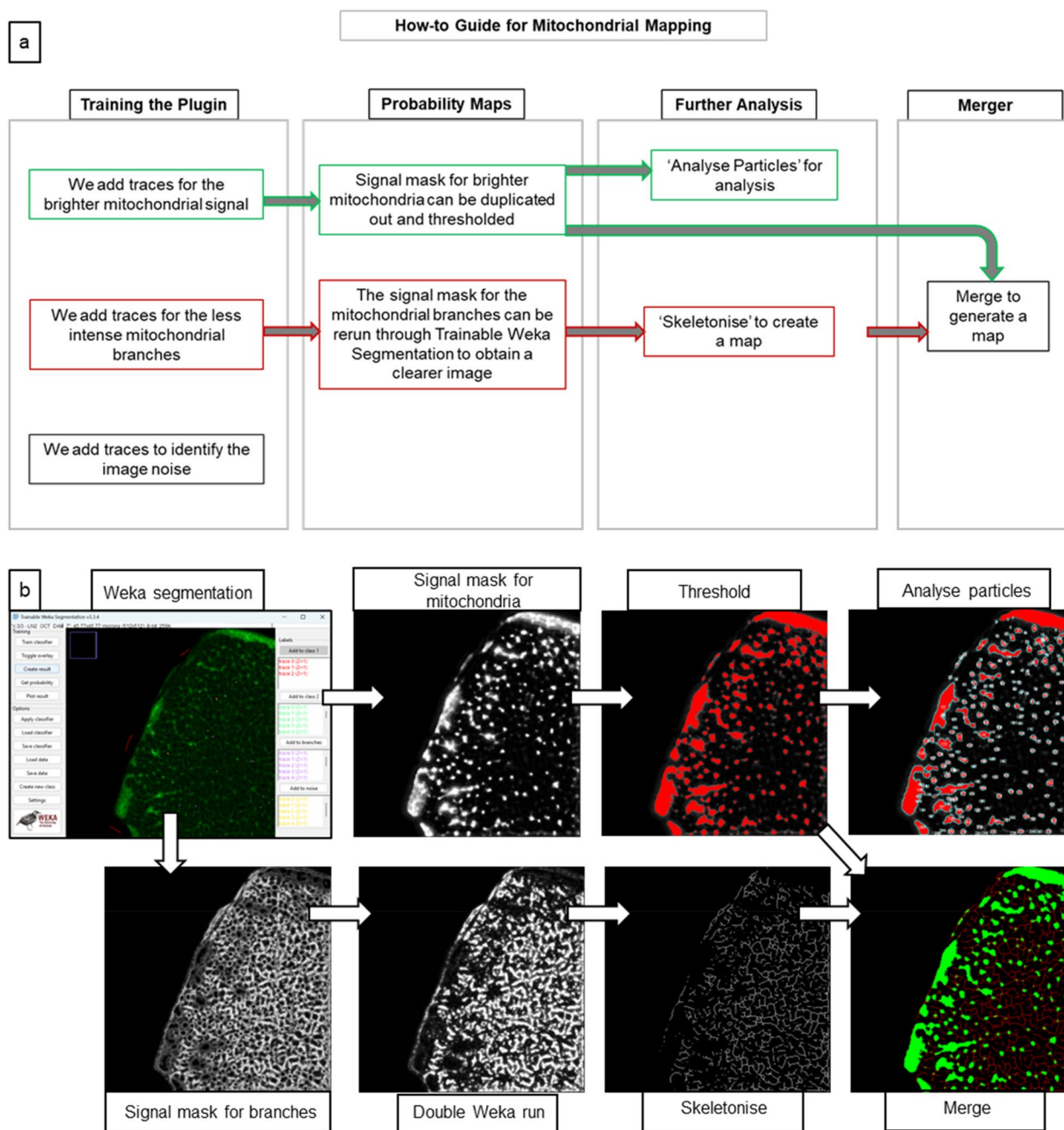


Fig. 14 Step-by-step instructions for creating a mitochondrial map using the described workflow. Detailed textual (a) and visual (b) description of each step in the mitochondrial mapping process utilising modification of our workflow employing the Trainable Weka Segmentation plugin

(See figure on next page.)

Fig. 15 Antibody penetration depth analysis. **a** Schematic illustration showing penetration of MitoView Green and DAPI across the entire thickness of the tissue section, with VDAC antibody restricted to the apical layer; **b** Colour-coded depth map generated using the temporal hyperstack function in Fiji, presenting the fluorescence emission intensity along the z-axis for samples permeabilised with either 0.25%, 0.5% Triton X-100, or PBT. The legend indicates the relation between colour and depth within the tissue sample, with yellow representing the region of greatest antibody/dye penetration and blue indicating areas of lesser penetration. Scale bar: 50 μ m

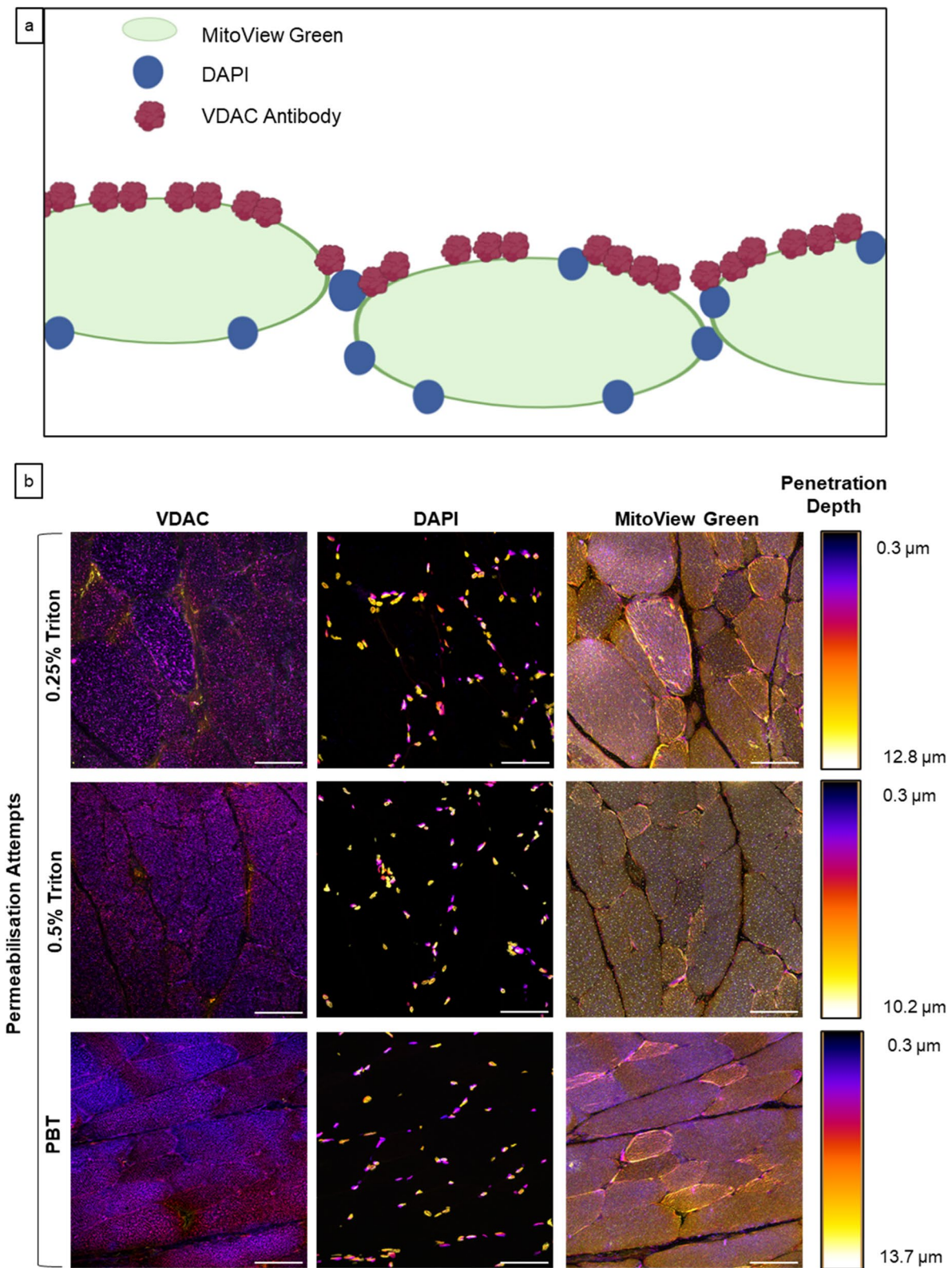


Fig. 15 (See legend on previous page.)

possibility of vapour formation and subsequent impeded cooling [7].

To mimic the conditions of human needle biopsies more closely, we opted to dissect the rat muscle into smaller fragments before subjecting them to various freezing methods. This approach allowed for a direct comparison of cryopreservation methods on biopsy-sized fragments, and their impact on tissue morphology and staining quality. Our histological staining results showed that varying degrees of ice crystal formation were observed in all samples, except for cryopreservation with pre-cooled isopentane with the sample placed in a histocassette (Fig. 5). Fluorescence microscopy demonstrated the same, with disruption of myofibrillar arrangement, saturation of fluorescence signal, and empty gaps dominating the tissue periphery of all samples except for isopentane/histocassette combination (Fig. 6). Previous literature demonstrates that isopentane offers enhanced tissue penetration with homogenous tissue freezing, resulting in consistent histological sections with minimal to no artefacts [5, 7], but scrutiny of our tissues revealed the presence of ice crystals in the peripheral regions. The use of histocassettes for containment during freezing, however, provided additional advantages in tissue handling. The use of containers with fenestra has been employed in some studies [6, 8]. A multi-hole cryovial employed by Huang et al. (2017) to freeze skeletal muscle samples demonstrated that fenestra around tissue promote flow of cryopreservative medium, and this limits the Leidenfrost effect seen with LN₂ [6]. Due to the lack of commercial availability of such vials, histocassettes were employed by Lee et al. (2020) when freezing rat muscle samples and human needle biopsies in LN₂ [8]. We decided to employ histocassettes for freezing in both LN₂ and pre-cooled isopentane. In contrast to the results shown by Lee et al., samples in histocassettes immersed in LN₂ exhibited ice crystals at the periphery of the specimen, with complete myofibrillar disruption observed using fluorescence microscopy. However, the use of histocassettes with pre-cooled isopentane resulted in no crystal artefacts on histological staining, and absolute preservation of myofibrillar arrangement on fluorescence microscopy. A further advantage of using histocassettes is the ability to label specimens for identification, and they are easily available in the laboratory settings. The histocassette samples allowed for more consistent handling after freezing, as their structure minimised the need for direct manipulation. Removal of the samples from the cassettes was easier, leading to less potential for damage compared to non-histocassette samples. This likely explains the reduced ice damage observed in the histocassette samples.

We utilised the OCT dip technique when freezing specimens with either LN₂ or pre-cooled isopentane,

aiming to take advantage of its cryoprotective properties while preserving tissue morphology. We also wished to assess any effects OCT may have on smaller tissue samples. Unfortunately, ice crystals were observed in muscle samples frozen in this way. This reaffirmed our previous findings with whole muscle samples (Fig. 3) and emphasised the drawbacks associated with OCT in the context of skeletal muscle cryopreservation.

Our experimental freezing setup for the smaller rat skeletal muscle samples consisted of simple and readily accessible equipment. With LN₂ in a dewar, and isopentane in a beaker mounted on a ladle, we provided a cost-effective and practical experimental setup that can easily be established by researchers in various laboratory settings and can be performed independently with ease.

We have also demonstrated PSR to be a useful tool in conjunction with H&E staining to provide robust evaluation of cryopreservation outcomes, and aid in selecting the most ideal methods (Fig. 5). If cryopreservation methods are optimised and result in tissue samples that exhibit preserved structural integrity, outcomes of subsequent experiments, such as fluorescence microscopy, can be considered reliable as tissues are free of crystal artefacts.

Having identified the isopentane/histocassette method as the most effective and reliable cryopreservation technique, we then focused on optimising the analysis of frozen skeletal muscle tissues. To this end, we developed and refined a workflow for mitochondrial analysis, aiming to overcome existing challenges and improving the clarity of mitochondrial imaging in skeletal muscle studies. We realised the lacunae that exist in the literature regarding mitochondrial analysis of confocal microscopy images of skeletal muscle tissues, with most platforms focusing specifically on cells. Here, we created and optimised a workflow adopting existing Fiji plugins, to allow for tissue quantification of mitochondria, while trying to limit the effect of the high background observed with mitochondrial dyes.

We employed existing workflows, functions, and plugins in Fiji for mitochondrial network quantification. Mitochondrial analyser and MiNA plugins provide a broad range of parameters for this purpose [11, 12]. However, the high signal-to-noise ratio observed in skeletal muscle tissues stained with MitoView Green limits the extent to which the entire mitochondrial network can be thresholded in these plugins (Fig. 11). The use of threshold optimisation in Mitochondrial Analyser, and any of the available preprocessing options presented in MiNA, are both unable to demarcate the dimmer mitochondrial branches in type I myofibres, and the entire network in the weakly stained type II myofibres. Deconvolution algorithms have

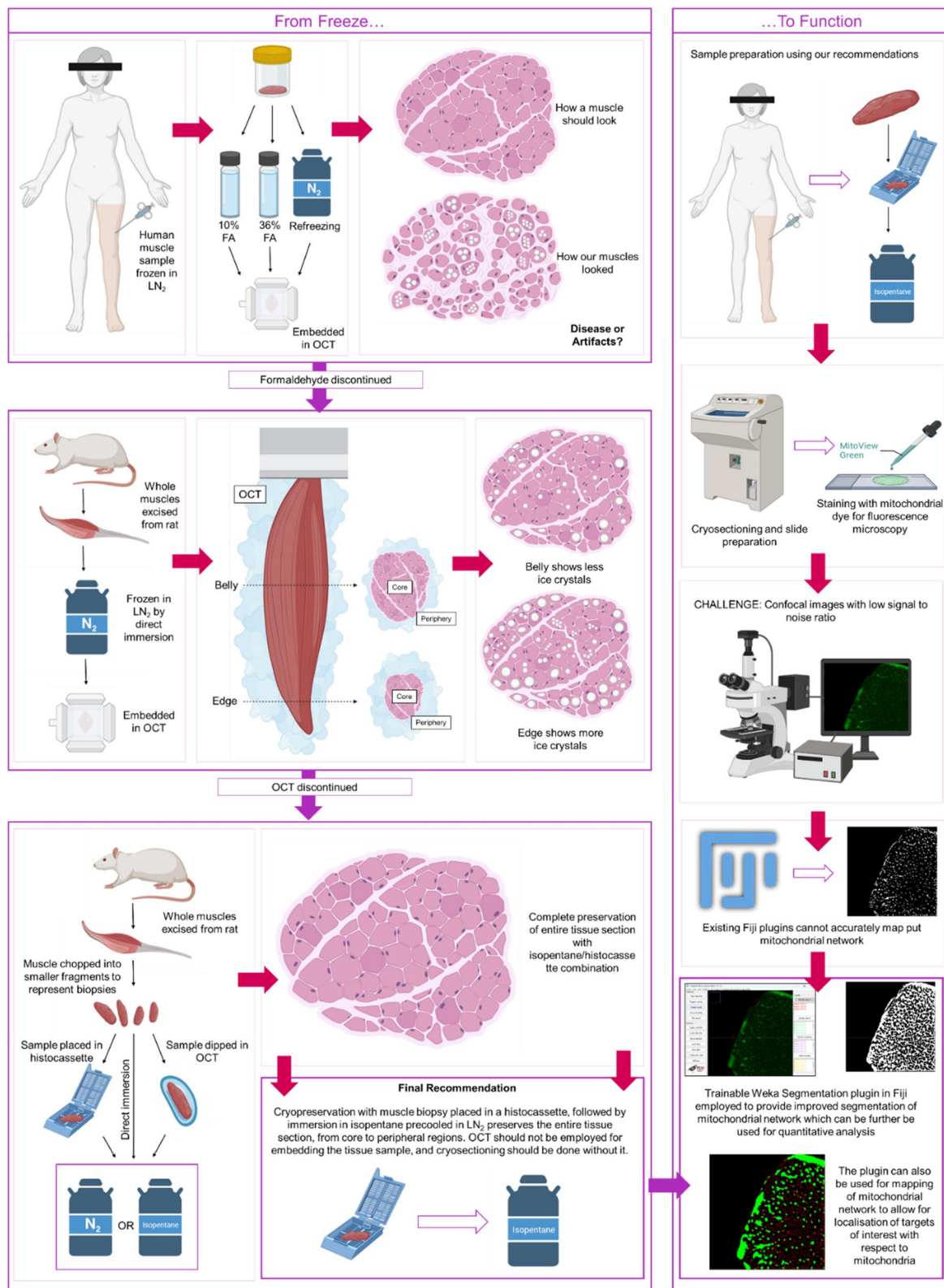


Fig. 16 Summary of optimised cryopreservation techniques and mitochondrial analysis workflow for skeletal muscle biopsies. The figure illustrates the key methodologies and findings of our study on cryopreservation of skeletal muscle biopsies, with final recommendation of use of isopentane/histocassette combination for snap-freezing. Mitochondrial analysis workflow adopting Trainable Weka Segmentation plugin is also highlighted

been employed in literature to enhance signal contrast and improve image resolution. However, deconvolution does not reduce the background and hence, does not allow for accurate distinction between signal and noise [12]. The use of Trainable Weka Segmentation plugin allows users to define the range of pixel intensities representing mitochondria and their branches, and to differentiate the network from the high tissue background. This will then allow for accurate mapping of mitochondria and thresholding of the image, which can be utilised for subsequent analysis. The Trainable Weka Segmentation plugin can accurately distinguish between signal (of all intensities) and noise, and can provide a map most closely aligned to the actual mitochondrial network. The overlaying option keeps the user in check to ensure additional features have not been falsely added to the image, nor been removed. The training data can be saved and reused for subsequent imaging analysis and can also be altered in case the new image shows variable signal-to-noise ratio, or presents different pixel intensities of the actual signal. The workflows employed in previous literature perform preprocessing that is unsuitable for type II myofibres, which stain very weakly with MitoView Green and present a significantly low signal-to-noise ratio. The Trainable Weka Segmentation plugin can be adequately trained to identify the dim signal in type II myofibres.

The modification of our workflow to generate a mitochondrial map presents an avenue to allow for localisation of our targets of interest with respect to spatial relationships within the mitochondrial network. We believe creating a ‘How To’ guide for the use of this plugin will be a helpful addition to support other researchers with their analysis needs. This can specifically aid in assessing fibre-specific changes in various conditions, and for proteins that have an association with mitochondrial networks.

The limitation of our mitochondrial analysis workflow is that it is time-consuming. However, this could be effectively streamlined if combined with more sophisticated coding and programming methods [40, 41]. Analysis requires thorough self-reflection to ensure no feature has been missed or falsely added, with effective blinding techniques in place to prevent bias at the analysis stage [42]. The variation in the intensity of signal across cells within the tissue section prevents the use of the same training data being applied to all sample sets.

One issue revealed in our study was the lack of penetration of VDAC antibodies in the tissue (Fig. 15). Fixation was not used as a method of preservation of tissues prior to cryosectioning, so epitope masking should potentially not arise. However, we will aim to perform antigen retrieval methods to assess whether the 10-min fixation

step during immunofluorescence is causing the penetration issue. Moreover, we will aim to use different skeletal muscle proteins to explore whether this is an antibody-specific effect, arising from the sensitivity of the antibody to fixation steps. For future studies, we plan to use Stimulated Emission Depletion (STED) microscopy as an alternative to obtain the highest resolution possible when measuring the depth of antibody diffusion distances.

In conclusion, our findings underscore the importance of selecting appropriate cryopreservation techniques to ensure the structural preservation of skeletal muscle biopsies, which is crucial for accurate histological and immunohistochemical analyses. The optimised workflow for mitochondrial analysis further enhances the utility of preserved tissue samples, providing a robust tool for future studies in muscle biology. A summary of the optimised cryopreservation techniques and workflow for mitochondrial analysis is shown in Fig. 16.

Supplementary Information

The online version contains supplementary material available at <https://doi.org/10.1186/s44330-024-00017-0>.

Supplementary Material 1.

Acknowledgements

Confocal imaging was conducted in The Robertson Trust Biophotonics Suite at University of Strathclyde. We thank Professor William Harnett (Strathclyde) for access to the EVOS cell imaging system, which is housed in his laboratory. Illustrations and schematics used in the manuscript were created with BioRender.com with figures exported under a paid subscription (PI: Dr Margaret Cunningham. Lab Licence Seat: Miss Maheen Wahid, University of Strathclyde).

Authors' contributions

Conceptualization MW, GG, EC, SG, JM and MRC devised the project; methodology; Experimental work, MW and GMack, LMR, JCG, SC, MRC; Data collection and formal analysis, MW, LMR; Writing - original draft preparation, MW, MRC; Writing - review and editing, all authors; Data visualization, MW, LMR, MRC, GG, GMcC; Supervision, MRC, GG, EC, SG, JM; Funding acquisition, MW, GG, MRC. All authors have read and approved the final manuscript.

Funding

MW is funded as a PhD student through the University of Strathclyde Faculty of Science Global Research Scholarship Programme (awarded 2023) Reference number 229057368. JM is funded by Medical Research Scotland PhD Reference PhD-50007-2-19. LMR is funded by Leverhulme Trust. The EVOS FL Auto microscope was purchased through a gift to the University of Strathclyde provided by Mr. Ken Wye Saw.

Data availability

The datasets generated and analysed during the current study are available in the Pure Data Repository, <https://doi.org/10.15129/81f66b7a-4a57-4426-a8aefc07e2affc38>.

Declarations

Ethics approval and consent to participate

The muscle biopsies from healthy human volunteers were collected as part of another study [15]. The samples were collected by Prof Stuart Gray, a co-author for both the current and cited study, and the use of these samples in the current study for microscopy analysis was ethically approved by the College of Medical, Veterinary and Life Sciences Ethical Committee at the

University of Glasgow (Approval No. 200150044). Participants provided written informed consent prior to participation in the original study. No additional ethics approval was required for the current study, as the use of the samples for microscopic analysis falls under the scope of the original ethical approval. Animal work was conducted in the Biological Procedures Unit at the Strathclyde Institute of Pharmacy and Biomedical Sciences (SIPBS), University of Strathclyde, Glasgow. The animals were housed in cages of up to 4 rats, within the Home Office Code of Practice Stocking Density, on a cycle of 12 h light/12 h dark, with access to standard chow diet and purified water. All animals were handled in strict accordance with good animal practice approved by The Animals in Science Regulation Unit. Each procedure was performed under sterile conditions and adapted by the Guide for the Care and Use of Laboratory animals published by the US National Institutes of Health (NIH Publication No. 85–23, revised 1996) and Directives 2010/63/EU of the European Parliament.

Consent for publication

Not applicable.

Competing interests

The authors declare no competing interests.

Author details

¹Strathclyde Institute for Pharmacy and Biomedical Sciences (SIPBS), University of Strathclyde, 161 Cathedral Street, Glasgow, UK. ²School of Medicine, Dentistry & Nursing, College of Medical, Veterinary and Life Sciences, University of Glasgow, Glasgow, UK. ³School of Cardiovascular and Metabolic Health, College of Medical Veterinary and Life Sciences, University of Glasgow, Glasgow, UK. ⁴Swansea University Medical School, Swansea University, Swansea, UK.

Received: 8 August 2024 Accepted: 25 October 2024

Published online: 02 December 2024

References

- Patel HP, White MC, Westbury L, Syddall HE, Stephens PJ, Clough GF, Cooper C, Sayer AA. Skeletal muscle morphology in sarcopenia defined using the ewgsp criteria: findings from the hertfordshire sarcopenia study (Hss). *BMC Geriatr*. 2015;15(1). <https://doi.org/10.1186/s12877-015-0171-4>.
- Joyce NC, Oskarsson B, Jin L-W. Muscle biopsy evaluation in neuromuscular disorders. *Phys Med Rehabil Clin N Am*. 2012;23(3):609–31. <https://doi.org/10.1016/j.pmr.2012.06.006>.
- Orsso CE, Montes-Ibarra M, Findlay M, Van Der Meij BS, De Van Der Schueren MAE, Landi F, Laviano A, Prado CM. Mapping ongoing nutrition intervention trials in muscle, sarcopenia, and cachexia: a scoping review of future research. *J Cachexia Sarcopenia Muscle*. 2022;13(3):1442–59. <https://doi.org/10.1002/jcsm.12954>.
- Newmire DE, Willoughby DS. The skeletal muscle micro biopsy method in exercise and sports science research: a narrative and methodological review. *Scand J Med Sci Sports*. 2022;32(11):1550–68. <https://doi.org/10.1111/sms.14215>.
- Meng H, Janssen PML, Grange RW, Yang L, Beggs AH, Swanson LC, Cossette SA, Frase A, Childers MK, Granzier H, Gussoni E, Lawlor MW. Tissue triage and freezing for models of skeletal muscle disease. *J Vis Exp*. 2014(89). <https://doi.org/10.3797/51586>.
- Huang Y, He M, Zeng Q, Li L, Zhang Z, Ma J, Duan Y. A Multi-Hole cryovial eliminates freezing artifacts when muscle tissues are directly immersed in liquid nitrogen. *J Vis Exp*. 2017(122). <https://doi.org/10.3791/55616>.
- Anwar S, Yokota T. Rapid freezing of skeletal and cardiac muscles using isopentane cooled with liquid nitrogen and tragacanth gum for histological, genetic, and protein expression studies. *Methods Mol Biol*. 2023:45–53. https://doi.org/10.1007/978-1-0716-2772-3_3.
- Lee CC, Hoang A, Segovia D, Herbst A, Barthelemy F, Gibbs E, Crosbie R, Nelson SF, Miceli C, Wanagat J. Enhanced methods for needle biopsy and cryopreservation of skeletal muscle in older adults. *J Cytol Histol*. 2020;11(2). <https://doi.org/10.37421/jch.2020.11.553>.
- Brand MD, Orr AL, Perevoshchikova IV, Quinlan CL. The role of mitochondrial function and cellular bioenergetics in ageing and disease. *Br J Dermatol*. 2013;169:1–8. <https://doi.org/10.1111/bjd.12208>.
- Schindelin J, Arganda-Carreras I, Frise E, Kaynig V, Longair M, Pietzsch T, Preibisch S, Rueden C, Saalfeld S, Schmid B, Tinevez J-Y, White DJ, Hartenstein V, Eliceiri K, Tomancak P, Cardona A. Fiji: an open-source platform for biological-image analysis. *Nat Methods*. 2012;9(7):676–82. <https://doi.org/10.1038/nmeth.2019>.
- Valente AJ, Maddalena LA, Robb EL, Morafi F, Stuart JA. A Simple imagej macro tool for analyzing mitochondrial network morphology in mammalian cell culture. *Acta Histochem*. 2017;119(3):315–26. <https://doi.org/10.1016/j.acthis.2017.03.001>.
- Hemel IMGM, Engelen BPH, Lubber N, Gerards M. A hitchhiker's guide to mitochondrial quantification. *Mitochondrion*. 2021;59:216–24. <https://doi.org/10.1016/j.mito.2021.06.005>.
- Biotium. Mitoview™ Mitochondrial Dyes: Fluorogenic mitochondrial stains for live cells that rapidly accumulate in mitochondria and can be imaged without washing. 2023. Available from: <https://biotium.com/product/mitoview-dyes/>.
- Sorvina A, Bader CA, Darby JRT, Lock MC, Soo JY, Johnson IRD, Caporale C, Voelcker NH, Stagni S, Massi M, Morrison JL, Plush SE, Brooks DA. Mitochondrial imaging in live or fixed tissues using a luminescent iridium complex. *Sci Rep*. 2018;8(1). <https://doi.org/10.1038/s41598-018-24672-w>.
- Alkhayl FFA, Ismail AD, Celis-Morales C, Wilson J, Radjenovic A, Johnston L, Welsh P, Sattar N, Gill JMR, Preston T, Gray SR. Muscle protein synthesis and muscle/metabolic responses to resistance exercise training in South Asian and White European Men. *Sci Rep*. 2022;12(1). <https://doi.org/10.1038/s41598-022-06446-7>.
- Wen W, Sun C, Chen Z, Yang D, Zhou Z, Peng X, Tang C. Alcohol Induces Zebrafish Skeletal Muscle Atrophy through Hmgb1/Tlr4/NF-κB Signaling. *Life*. 2022;12(8):1211. <https://doi.org/10.3390/life12081211>.
- Eltoum I, Fredenburgh J, Myers RB, Grizzle WE. Introduction to the Theory and Practice of Fixation of Tissues. *J Histotechnol*. 2001;24(3):173–90. <https://doi.org/10.1179/his.2001.24.3.173>.
- Cotta A, Carvalho E, da-Cunha-Júnior AL, Valicek J, Navarro MM, Junior SB, da Silveira EB, Lima MI, Cordeiro BA, Cauhi AF, Menezes MM, Nunes SV, Vargas AP, Neto RX, Paim JF. Muscle Biopsy essential diagnostic advice for pathologists. *Surg Exp Pathol*. 2021;4(1):3. <https://doi.org/10.1186/s42047-020-00085-w>.
- Fan C, Pirri C, Fede C, Guidolin D, Biz C, Petrelli L, Porzionato A, Macchi V, De Caro R, Stecco C. Age-related alterations of hyaluronan and collagen in extracellular matrix of the muscle spindles. *J Clin Med*. 2021;11(1):86. <https://doi.org/10.3390/jcm11010086>.
- Gaspar BL, Vasishtha RK, Radotra BD. Myopathology: a practical clinico-pathological approach to skeletal muscle biopsies. Singapore: Springer Singapore; 2019. Available from: <https://doi.org/10.1007/978-981-13-1462-9>.
- Riegman PHJ. Tissue preservation and factors affecting tissue quality. 2nd ed. Switzerland: Springer International Publishing; 2021. Available from: <https://doi.org/10.1007/978-3-030-55901-4>.
- Rogers GL, Hoffman BE. Optimal Immunofluorescent Staining for Human Factor Ix and Infiltrating T Cells Following Gene Therapy for Hemophilia B. *J Genet Syndr Gene Ther*. 2012;S1. <https://doi.org/10.4172/2157-7412.s1-012>.
- Dubowitz V, Sewry CA, Oldfors A. Muscle Biopsy: A Practical Approach. 5th ed. London: Elsevier; 2020. Available from: <https://www.sciencedirect.com/book/9780702043406/muscle-biopsy-a-practical-approach>.
- Sabel MS. Chapter 3 - the Breast Mass, Breast Biopsies, and Benign Lesions of the Breast. In: Sabel MS, editor. *Essentials of Breast Surgery*. Philadelphia: Mosby; 2009. p. 41–65. Available from: <https://doi.org/10.1016/B978-0-323-03758-7.X0001-4>.
- Ogata T, Yamasaki Y. Ultra-High-Resolution Scanning Electron Microscopy of Mitochondria and Sarcoplasmic Reticulum Arrangement in Human Red, White, and Intermediate Muscle Fibers. *Anat Rec*. 1997;248(2):214–23. [https://doi.org/10.1002/\(sici\)1097-0185\(199706\)248:2%3c214::aid-ar8%3e3.0.co;2-s](https://doi.org/10.1002/(sici)1097-0185(199706)248:2%3c214::aid-ar8%3e3.0.co;2-s).
- Jackman MR, Willis WT. Characteristics of Mitochondria Isolated from Type I and Type IIB Skeletal Muscle. *Am J Physiol Cell Physiol*. 1996;270(2):C673–C8. <https://journals.physiology.org/doi/abs/10.1152/ajpcell.1996.270.2.C673>.
- Arganda-Carreras I, Kaynig V, Rueden C, Eliceiri KW, Schindelin J, Cardona A, Sebastian SH. Trainable Weka Segmentation: a machine learning tool for microscopy pixel classification. *Bioinformatics*. 2017;33(15):2424–6. <https://doi.org/10.1093/bioinformatics/btx180>.

28. Leonard AP, Cameron RB, Speiser JL, Wolf BJ, Peterson YK, Schnellmann RG, Beeson CC, Rohrer B. Quantitative analysis of mitochondrial morphology and membrane potential in living cells using high-content imaging, machine learning, and morphological binning. *Biochim Biophys Acta*. 2015;1853(2):348–60. <https://doi.org/10.1016/j.bbamcr.2014.11.002>.
29. Johnson ML, Robinson MM, Nair KS. Skeletal muscle aging and the mitochondrion. *TEM*. 2013;24(5):247–56. <https://doi.org/10.1016/j.tem.2012.12.003>.
30. Ignatieva E, Smolina N, Kostareva A, Dmitrieva R. Skeletal muscle mitochondria dysfunction in genetic neuromuscular disorders with cardiac phenotype. *Int J Mol Sci*. 2021;22(14):7349. <https://doi.org/10.3390/ijms22147349>.
31. Rygiel KA, Picard M, Turnbull DM. The ageing neuromuscular system and sarcopenia: a mitochondrial perspective. *Physiol J*. 2016;594(16):4499–512. <https://doi.org/10.1113/JP271212>.
32. Lundby C, Jacobs RA. Adaptations of skeletal muscle mitochondria to exercise training. *Exp Physiol*. 2016;101(1):17–22. <https://doi.org/10.1113/EP085319>.
33. Esper ME, Kodippili K, Rudnicki MA. Immunofluorescence labeling of skeletal muscle in development, regeneration, and disease. *Methods Mol Biol*. 2023;113–32. https://doi.org/10.1007/978-1-0716-2675-7_9.
34. Guerin CJ. Using Antibodies in Microscopy: A guide to immunohistochemistry, part 2: ihc staining protocols. *Micros Today*. 2023;31(3):34–9. <https://doi.org/10.1093/mictod/qaad029>.
35. Snapes E, Astrin JJ, Bertheussen Krüger N, Grossman GH, Hendrickson E, Miller N, Seiler C. Updating international society for biological and environmental repositories best practices, Fifth Edition: a new process for relevance in an evolving landscape. *Biopreserv Biobank*. 2023;21(6):537–46. <https://doi.org/10.1089/bio.2023.0140>.
36. Mendy M, Caboux E, Lawlor RT, Wright J, Wild CP. Common minimum technical standards and protocols for biobanks dedicated to cancer research. Lyon (France): international agency for research on cancer; 2017. Available from: <https://pubmed.ncbi.nlm.nih.gov/33539055/>.
37. Chang T, Zhao G. Ice Inhibition for cryopreservation: materials, strategies, and challenges. *Adv Sci*. 2021;8(6):2002425. <https://doi.org/10.1002/adv.202002425>.
38. Baker MJ, Denton TT, Herr C. An explanation for why it is difficult to form slush nitrogen from liquid nitrogen used previously for this purpose. *Cryobiology*. 2013;66(1):43–6. <https://doi.org/10.1016/j.cryobiol.2012.10.007>.
39. Kumar A, Accorsi A, Rhee Y, Girgenrath M. Do's and Don'ts in the preparation of muscle cryosections for histological analysis. *J Vis Exp*. 2015;99:e52793. <https://doi.org/10.3791/52793-v>.
40. Valente A, Stuart J. 211 - a Generalized image workflow for quantitative analysis of mitochondrial networks. *Free Radic Biol Med*. 2017;112:147. <https://doi.org/10.1016/j.freeradbiomed.2017.10.224>.
41. Bosch A, Calvo M. automated quantitative analysis of mitochondrial morphology. *Methods Mol Biol*. 2019:99–115. https://doi.org/10.1007/978-1-4939-9686-5_6.
42. Holman L, Head ML, Lanfear R, Jennions MD. Evidence of experimental bias in the life sciences: why we need blind data recording. *PLoS Biol*. 2015;13(7):e1002190. <https://doi.org/10.1371/journal.pbio.1002190>.

Publisher's Note

Springer Nature remains neutral with regard to jurisdictional claims in published maps and institutional affiliations.